Cytosolic MONODEHYDROASCORBATE REDUCTASE 2 promotes oxidative stress signaling in Arabidopsis

Dongdong Xu, Lug Trémulot, Zheng Yang, Amna Mhamdi, Gilles Châtel-Innocenti, Laura Mathieu, Christophe Espinasse, Frank van Breusegem, Hélène Vanacker, Emmanuelle Issakidis- Bourguet, et al.

Cytosolic MONODEHYDROASCORBATE REDUCTASE 2 promotes oxidative stress signaling in Arabidopsis

Dongdong Xu[1*], Lug Trémulot[1*], Zheng Yang[1§], Amna Mhamdi[2,3], Gilles Châtel-Innocenti[1], Laura Mathieu[1§], Christophe Espinasse[1], Frank Van Breusegem[2,3], Hélène Vanacker[1], Emmanuelle Issakidis-Bourguet[1], Graham Noctor[1,4+]

[1]Institut des Sciences des Plantes de Paris-Saclay, Unité Mixte de Recherche 8618 Centre National de la Recherche Scientifique, Université de Paris-Saclay, 91190 Gif-sur-Yvette, France

[2]Department of Plant Biotechnology and Bioinformatics, Ghent University, 9052 Ghent, Belgium

[3]Center for Plant Systems Biology, VIB, 9052 Gent, Belgium

[4]Institut Universitaire de France (IUF), France

ORCID ID: 0000-0001-9959-1362 (A.M.), 0000-0002-3147-0860 (F.V.B.), 0000-0003-1980-4554 (G.N.)

*These authors contributed equally to this work

+ Correspondence: graham.noctor@universite-paris-saclay.fr

[§]Current addresses:

ZY: 20 Fute North Road, Shanghai, China (WuXi AppTec Co., Ltd. Biotech Unit)

LM: PHIM Plant Health Institute, Univ Montpellier, INRAE, CIRAD, Institut Agro, IRD, Montpellier, France

Statistics

Summary: 191 words

Introduction: 834 words

Materials and Methods: 1424 words

Results: 1514 words

Discussion: 2485 words

References: 75

Summary

The antioxidative enzyme monodehydroascorbate reductase (MDHAR) is represented by five genes in Arabidopsis, including four that encode cytosolic and peroxisomal proteins. The *in planta* importance of these specific isoforms during oxidative stress remain to be characterized. T-DNA mutants for *MDAR* genes encoding cytosolic and peroxisomal isoforms were studied. To examine their roles in conditions of intracellular oxidative stress, mutants were crossed with a *cat2* line lacking the major leaf catalase. Enzyme assays in *mdar* mutants and of recombinant MDHARs suggest that peroxisomal MDHAR1 and cytosolic MDHAR2 are major players in leaf NADH- and NADPH-dependent activities, respectively. All mutants showed a wild-type phenotype when grown in standard conditions. In the *cat2* background, loss of peroxisomal MDHAR functions decreased growth whereas loss of the cytosolic MDHAR2 function had no effect on growth but annulled a large part of transcriptomic and phenotypic responses to oxidative stress. The effects of the *mdar2* mutation included decreased salicylic acid accumulation and enhanced glutathione oxidation, and were reverted by complementation with the *MDAR2* sequence. Together, the data show that the cytosolic MDHAR2 is dispensable in optimal conditions but essential to promote biotic defence responses triggered by oxidative stress.

Key words

Antioxidants; ascorbate; catalase; glutathione; oxidative stress; pathogenesis-related (PR); salicylic acid

Introduction

Ascorbate is an essential compound in plants with several functions as an antioxidant and enzyme co-factor (Dowdle *et al*., 2007; Conklin *et al*., 2024). As an antioxidant, ascorbate reacts chemically with certain reactive oxygen species (ROS) and is a reductant for ascorbate peroxidase (APX; Conklin *et al*., 2024; Foyer & Kunert, 2024). APX is one of a battery of plant enzymes that counter excessive accumulation of H_2O_2 and avoid formation of its more reactive derivatives: others include various other types of peroxidases as well as catalase (Davletova *et al*., 2005; Mhamdi *et al*., 2010b).

Continued function of APX requires effective regeneration of ascorbate from its oxidized forms. The first oxidation product is monodehydroascorbate (MDHA), an unstable free radical that can be directly reduced back to ascorbate (Foyer & Kunert, 2024). A second fate is chemical dismutation, in which two MDHA molecules produce one molecule each of ascorbate and dehydroascorbate (DHA), a form that is both more oxidized and more stable than MDHA. While ascorbate and DHA can be readily quantified in tissue extracts, specialized equipment is required to detect MDHA and very little quantitative data are available. However, it has been reported that MDHA signals are enhanced in response to oxidative stress (Veljovic-Jovanovic *et al*., 1998) and kinetic modelling of the response to increased H_2O_2 concentrations suggests that MDHA will increase as ascorbate oxidation accelerates (Tuzet *et al*., 2019).

Reductases that can convert MDHA and DHA to ascorbate have been known for many years. While DHA reductase (DHAR) uses glutathione as reductant, MDHA reductase (MDHAR) is a flavoprotein that functions with NADH or NADPH as a co-factor (Foyer & Halliwell, 1977; Hossain & Asada, 1984, 1985; Hossain *et al*., 1984; Sano *et al*., 1995). Both enzymes are encoded by several genes in plants. Recent studies have examined the roles of specific DHAR isoforms using loss-of-function Arabidopsis mutants (Noshi *et al*., 2017; Rahantaniaina *et al*., 2017; Terai *et al*., 2020; Hamada *et al*., 2023). One observation is that knocking out both cytosolic DHAR isoforms abolishes a large part of the glutathione oxidation triggered by oxidative stress in *cat2*, an effect accompanied by compromised induction of the salicylic acid (SA) pathway (Rahantaniana et al., 2017). Compared to DHAR, less information is available for specific mutants for *MDAR*. Engineering altered expression of *MDAR* has been reported to influence both ascorbate contents and stress tolerance (El Airaj *et al*., 2013; Gest *et al*., 2013), but systematic comparisons of the roles of the different isoforms in response to oxidative stress are lacking.

In Arabidopsis, five *MDAR* genes encode MDHAR proteins located in various compartments. While *MDAR1* and *MDAR4* encode proteins associated with peroxisomes, *MDAR2* and *MDAR3* encode cytosolic enzymes (Lisenbee *et al*., 2005; Eastmond, 2007). A single gene, *MDAR5/6*, codes for proteins that are addressed to both mitochondria and chloroplasts (Chew *et al*., 2003). As well as activities located in these compartments, several other systems can also reduce MDHA to ascorbate. These include ferredoxin in the chloroplast, an MDHAR activity located at the plasma membrane, a tonoplast ascorbate-dependent type b cytochrome, and 12-oxo-phytodieonic acid reductase 3 (Miyake & Asada, 1994; Bérczi & Møller, 1998; Maynard *et al*., 2020; Gradagna *et al*., 2023).

Given the presence of these numerous MDHA-reducing systems, questions remain concerning the importance of each in given conditions. The peroxisome-associated MDHAR4 has been shown to be required for optimal post-germinative growth, probably linked to metabolism of H_2O_2 produced during metabolism of seed storage lipids (Eastmond, 2007). In contrast to this classical antioxidant function, the mitochondrial MDHAR5 has been implicated in sensitizing plants to the xenobiotic TNT, and evidence was presented that this occurs through catalysis of ROS production (Johnston *et al*., 2015). This last observation is a striking example of the possible pro-oxidant functions that so-called recognized antioxidative enzymes might exert in certain conditions (Noctor, 2015).

Loss-of-function mutants for the five Arabidopsis *MDAR* genes do not show a marked phenotype relative to the wild-type when grown in standard conditions (Tanaka *et al*., 2021). This is in line with many other studies of genes encoding antioxidative enzymes, and highlights the redundancy built in to the complex ROS-processing network. In the present report, we confirm these observations for *mdar* mutants grown in our conditions, but we also analyse the roles of MDHARs under conditions where increased H_2O_2 availability causes ascorbate metabolism to turn over more rapidly. For this, we introduced mutations for the peroxisomal and cytosolic isoforms into a catalase-deficient background (*cat2*; Yang *et al*., 2019). The interest of the *cat2* system is that increased H_2O_2 availability occurs through the photorespiratory pathway and can be sustained inside the cell, placing an increased load on antioxidative pathways and mimicking environmentally induced oxidative stress (Mhamdi *et al*., 2010a; Tuzet *et al*., 2019). Our findings reveal an important role for the cytosolic MDHAR2 in these conditions. Intriguingly, disabling the expression of this enzyme weakens rather than aggravates downstream responses triggered by the *cat2* mutation. This suggests that in addition to its antioxidant function, MDHAR2 can promote certain outcomes of oxidative stress.

Materials & Methods

Plant materials and growth

Arabidopsis mutants used in this study were in the Columbia genetic background, and all seeds were obtained from the Nottingham Arabidopsis Stock Centre (http://nasc.nott.ac.uk). Lines carrying T-DNA insertions in the *MDAR1*, *MDAR2*, *MDAR3*, and *MDAR4* genes were identified using insertion mutant information obtained from the SIGnAL Web site (http://signal.salk.edu). For further information, see Supporting Information Figure S1a. The *cat2* mutant was *cat2-1* (Queval *et al*., 2009). Double mutants were produced by crossing. After verification of heterozygotes in F1 plants by PCR, double homozygotes were identified similarly in the F2 generation (Fig. S1b).

Seeds were firstly germinated in 0.5 MS medium containing 1% sucrose. After seven days, plants were transferred to soil (Tref terreau P1, Jiffy France SARL, Trevoux, France) and grown in a controlled-environment growth chamber in a 16 h photoperiod and an irradiance of 200 µmol. m^{-2} s^{-1} at leaf level, 20 °C/18 °C, 65 % humidity, and given nutrient solution twice per week (Plant-prod 14-12-32, 280 g/L and Fertiligo 4.35 mL/L). Unless otherwise stated, plants were sampled after three weeks growth. Samples were rapidly frozen in liquid nitrogen and stored at −80 °C until analysis. All data are means ± SE of at least three biological replicates obtained from different plants, and experiments were repeated at least twice.

Plasmid constructs and plant transformation

The full-length cDNA of Arabidopsis *MDAR2* was amplified on total cDNA from Col-0 and GFP and T35S sequences were amplified on the pH7FWG2 plasmid using the primers in Supporting Information Table S1. Then, the three fragments and pH7FWG2 plasmid opened with SpeI and XbaI restriction enzymes were assembled using the HiFi DNA Assembly Master Mix (New England BioLabs) according to the manufacturer's instructions. Two constructs were done, to obtain *MDAR2* fused to GFP in N-terminal or C-terminal, driven by the 35S promoter of the Cauliflower mosaic virus. Purified plasmids were analyzed and sequenced to confirm successful fusion constructs. Agrobacterium tumefaciens strain GV3101 pMP90 (Koncz & Schell, 1986) was transformed with confirmed binary vector constructs (Höfgen & Willmitzer, 1988) and used to transform developing floral tissues of *cat2 mdar2* by the floral dip method (Clough & Bent, 1998).

Recombinant protein production and purification

MDAR1 and *MDAR2* cDNA sequences were amplified from total cDNA from Col-0 with the primers in Supporting Information Table S1, and then cloned into the pGENI vector (Bohrer *et al*., 2012) opened with *Nco*I and *Xho*I restriction enzymes, using the HiFi DNA Assembly Master Mix (New England BioLabs). Recombinant protein production and strep tag-based purification were performed as described in detail by Vanacker *et al*. (2018). Purity and molecular mass of the proteins were checked by SDS-PAGE with Coomassie blue staining. Protein concentrations were determined spectrophotometrically at 450 nm, corresponding to the flavin adenine nucleotide (FAD) absorption peak, using a molar extinction coefficient of 11.3 mM^{-1} cm^{-1} (Aliverti *et al*., 1999). The purified protein was stored at -80°C until use.

Transcriptomic analysis

For RNA sequencing, three biological replicates were used, each consisting of 100 mg leaf tissue from different plants. Samples were extracted using Spectrum™ Plant Total RNA Kit (SIGMA, Germany), and treated with DNase during RNA purification. Library preparation and sequencing were performed at the Nucleomics Core (VIB, Leuven, Belgium), using TruSeq Stranded mRNA Library Preparation Kit (Illumina). Samples were sequenced on IlluminaNextseq 500 (75-bp single-end reads), and reads were aligned to the Arabidopsis genome by STAR (v 2.5.2b) (Dobin *et al*., 2013) using the Araport11 annotation (Cheng *et al*., 2017). The number of reads per gene was quantified with the featureCounts function as implemented in the Subread package v 1.6.2 (Liao *et al*., 2014). Genes with less than 5 reads in at least three samples were excluded for further analysis. Differentially expressed genes (DEGs) determination was conducted using the DiCoExpress (Lambert *et al*., 2020) with FDR<0.01 and a |log2FC|>1 as threshold. Hierarchical clustering was performed on DEGs using the hclust function using “ward.D2” method with a distance matrix based on Pearson correlation coefficients (R Core Team, 2021). The heatmap was generated using ComplexHeatmap package v 2.12.1 (Gu *et al*., 2016). The Gene Ontology enrichment analysis for the 4 clusters was performed using clusterProfiler v 4.4.4 with a p-value<0.05 cutoff (Xu *et al*., 2024). A list of DEGs is presented in Supporting Information Table S2.

Subcellular localization and genetic complementation

Seedlings of the *cat2 mdar2* mutant were selected for stable transformation with GFP-*MDAR2* or *MDAR2*-GFP. Transformed T1 seeds were germinated on agar and identified based on their resistance to hygromycin or screened using a Leica (Deerfield, IL) dissecting microscope equipped

with a mercury lamp and epifluorescence filter set (Karimi *et al*., 2002). Resistant and PCR-positive transgenic plants were transferred to a growth chamber and maintained up to the T2 generation, when segregation analysis was performed on complemented *cat2 mdar2* lines. Two independent complemented lines were selected and used for analysis. Confocal microscopy was performed as in Rahantaniaina *et al*. (2017). For immunoblotting, proteins from complementation lines were extracted using TBS 1x buffer with added protease inhibitor, as previously described, with 500 µL per extract. Protein quantification was performed using the Bradford assay. A TGX stain-free gel and PVDF membrane system were used (BIO-RAD). To detect the GFP-MDHAR2 fusion protein, the PVDF membrane was incubated in a primary anti-GFP antibody (rabbit, diluted 1:5000) from Abcam for over-night at 4°C, followed by a secondary anti-rabbit antibody (diluted 1:10000) incubation for two hours at room temperature.

Immunoprecipitation–mass spectrometry (IP-MS) analysis

IP-MS analysis of *cat2 mdar2* MDAR2-GFP lines was performed using three biological triplicates as previously described (Wendrich *et al*., 2017) and *cat2* as a background control. Briefly, around three grams of leaf material were ground in liquid nitrogen and homogenised in extraction buffer containing 50 mM Tris–HCl, pH 7.5, 0.15M NaCl, 1 protease inhibitor tablet/50 ml (Roche) and 1% (v/v) NP40. Protein extracts were sonicated, diluted to remove excess of NP40, and then centrifuged twice for 15 min at 42 000 *g*. Extracts were incubated for 2 h with anti-GFP-coated microbeads (µMACS; Miltenyi), applied on the µColumns (µMACS; Miltenyi), washed and eluted with preheated ammonium bicarbonate buffer. To prepare samples for MS analysis, the 50 µL eluent was reduced with dithiothreitol, alkylated with iodoacetamide and digested with sequencing-grade Trypsin. The digested samples were purified using the Bond Elut OMIX tips (Agilent Technologies) and analysed by liquid chromatography–tandem mass spectrometry with a UltiMate™ 3000 RSLCnano System connected to LTQ Orbitrap Velos mass spectrometer (Thermo Fisher Scientific). The resulting raw data were analysed in label-free quantification mode using MaxQuant software (1.6.9.0) as reported by He *et al*. (2021). "ProteinGroups" file from MaxQuant was further analysed using an *in house* R-script based tool to perform statistical analyses as described in Schippers *et al*. (2024). The list of identified proteins, enrichment ratios and statistics are given in Supporting Information Table S3. *In silico* subcellular localisation of immunoprecipitated proteins was determined using SUBA5 (https://suba.live/; Hooper *et al*., 2022). Based on the known subcellular localization of MDHAR2, annotated mitochondrial, plastidial, and apoplastic proteins were omitted from further analysis. The candidate interacting proteins were filtered for an enrichment ratio >25 and an adjusted *p*-value<0.05. Biological process was assigned to each protein based on its annotation on Thalemine

(https://bar.utoronto.ca/thalemine/; Pasha *et al*., 2020). The interaction networks were generated using Cytoscape 3.10.2 (Shannon *et al*., 2003) and the application "Autoannotate" (https://apps.cytoscape.org/apps/autoannotate).

Transcript quantification by RT-qPCR

Total RNA was extracted with the NucleoSpin RNA Plant and Fungi kit (Macherey-Nagel) following the manufacturer's instructions. RNA quality was determined by gel electrophoresis and concentration estimated using a nanodrop spectrophotometer at 260 nm. Reverse transcription and first-strand cDNA synthesis were performed using the ImProm-II™ Reverse Transcriptase (Promega). qPCR was performed according to Queval *et al*. (2009). Transcripts were quantified relative to those of *ACTIN2* and *PP2A* or *ACTIN2* and *UBIQUITIN*. Primer sequences are listed in Supporting Information Table S1.

Other analyses

MDHAR activities were measured according to protocols detailed in Noctor *et al*. (2016), by monitoring oxidation of NADH or NADPH in the presence of ascorbate and ascorbate oxidase at 340 nm. Oxidized and reduced forms of glutathione and ascorbate were measured by plate-reader assay as described by Queval & Noctor (2007). Briefly, ascorbate was measured as the removal of A_{256} in the presence of ascorbate oxidase and glutathione was measured as the NADPH- and GR-dependent increase in A_{412} as a result of reduction of DTNB. A detailed procedure has been recently published (Noctor and Mhamdi, 2022). Total SA was measured by HPLC-fluorescence, according to the protocol of Chaouch *et al*. (2010). Percentage lesion area on rosette leaves was quantified using ImageJ software.

Results

As a first step to exploring the roles of MDHAR isoforms in Arabidopsis, we characterised gene-specific mutants for the two cytosolic (MDHAR2 and MDHAR3) and two peroxisome-associated (MDHAR1 and MDHAR4) enzymes. Transcript abundance analysis showed that all four mutants were knockouts or severe knockdowns and that effects were specific to each gene (Fig. 1a). However, with the exception of some delayed early growth in *mdar4* that could be overcome by germinating plants on agar medium containing sucrose (Eastmond, 2007), all plants showed a phenotype similar to wild-type, with little effect on rosette size (Fig. S2). Enzyme assays revealed that total extractable leaf NADH-dependent MDHAR activity was substantially decreased in *mdar1* but not in *mdar2*, *mdar3*, or *mdar4* (Fig. 1b). The NADPH-dependent activity was decreased in *mdar1* and *mdar2*, but unaffected in the other two lines (Fig. 1b). None of the mutations had a detectable impact on leaf ascorbate or glutathione status, both of which remained largely reduced (Fig. 1c,d). This suggests that, in standard conditions, where the ascorbate-glutathione pathway is turning over relatively slowly, none of the MDHAR isoforms are irreplaceable for growth and development.

Based on the activities observed in the mutants, MDHAR1 and MDHAR2 are the major players in leaves, albeit with different contributions to the NADH- and NADPH-dependent activities. To investigate this point further, the two enzymes were purified as recombinant proteins and their affinities for the two reductant cofactors were determined. Examples of kinetic curves are shown in Supporting Information Figure S3 and the data are summarized in Table 1. While both enzymes showed a greater catalytic efficiency for NADH compared to NADPH, the difference was much less marked for MDHAR2. While K_{cat} was over 100-fold greater for NADH compared with NADPH in the case of MDHAR1, the difference was only 6-fold for MDHAR2 (Table 1; Fig. S3).

As a first step to analysing the importance of the different MDHARs in oxidative stress conditions, we compared how their expression was modified in the oxidative stress line, *cat2*, in which catalase deficiency places an enhanced demand on reductive pathways of H_2O_2 metabolism. A survey of the enzymes involved in major H_2O_2-metabolising pathways (Fig. S4) revealed (1) that *CAT1* and *CAT3* showed little compensatory effect in response to *CAT2* deficiency; (2) that genes encoding cytosolic proteins were most strongly induced, with those encoding enzymes found in the peroxisomes or chloroplast being less or not at all affected; and (3) that cytosolic enzymes of the ascorbate-glutathione pathway (APX1, MDHAR2, MDHAR3, DHAR2, GR1) were up-regulated alongside cytosolic peroxiredoxins and several glutathione peroxidase-like enzymes (Fig. S4). We further analysed the responses of the four *MDAR* genes to oxidative stress using RT-qPCR. This analysis largely confirmed

the inducibility of the cytosolic isoforms in response to intracellular oxidative stress (Fig. 2a). Induction of these two forms was accompanied by enhanced MDHAR activity in *cat2*, an effect that was stronger with NADPH than NADH (Fig. 2b).

To examine the role of the different MDHARs in oxidative stress conditions more directly, each of the mutations was introduced into the *cat2* background to produce double mutants that lacked both most of the leaf catalase activity and one of the MDHAR isoforms. The mutations produced similar effects on the expression of the different *MDAR*s in the *cat2* background to those observed in the Col-0 background (Fig. S5); ie, each mutation had a strong specific effect on the respective transcript without producing accompanying or compensatory effects on expression of the other *MDAR* genes. Neither *mdar3* nor *mdar4* affected the *cat2*-enhanced MDHAR activity. Most of the NADPH-dependent activity was removed by *mdar2* (Fig. 3a) while the NADH-dependent activity was decreased in both *mdar1* and, to a lesser extent, *mdar2* (Fig. 3a). Assays of ascorbate and glutathione in the *cat2* background revealed that *mdar2* produced significant effects on these antioxidant pools: while the effect on reduced ascorbate was slight (Fig. 3b), a larger impact on glutathione was observed, with the *mdar2* mutation further increasing the accumulation of total and oxidized glutathione observed in *cat2* (Fig. 3c).

The *cat2* mutation triggers two phenotypic effects. First, rosette growth is decreased compared to Col-0. Second, lesions that are similar to those observed in the hypersensitive response to pathogens appear spontaneously on the leaves (Chaouch *et al*., 2010). Phenotypic analysis of growth in the double mutants revealed differential effects of the *mdar* mutations on these two effects: while the *cat2*-triggered decrease in growth was exacerbated in *cat2 mdar1* and *cat2 mdar4*, *cat2 mdar2* showed much fewer lesions than *cat2* and the other double mutants (Fig. 4a,b). Since the *cat2* lesion phenotype is associated with and dependent on SA accumulation (Chaouch et al., 2010), this phytohormone was quantified, revealing (1) that the single *mdar2* mutants showed similarly low SA contents to those observed in the wild-type and (2) that the enhanced SA contents in *cat2* were largely abolished in *cat2 mdar2* (Fig. 4c). Analyses of the expression of SA marker genes (*PR1*, *PR2*, *PR5*) and *ICS1*, encoding a key enzyme in SA synthesis, produced a similar pattern; ie, induction of the SA markers in *cat2* was strongly decreased by the presence of the *mdar2* mutation but less so by loss of the other *MDAR* functions (Fig. 4d).

The effects of the *mdar2* mutation on *cat2*-triggered SA signalling recall those reported in previous studies in which other components of the ascorbate-glutathione pathway were disabled, notably observations in a *cat2 dhar1 dhar2 dhar3* quadruple mutant, in which all three DHAR-encoding gene

functions are lost (Rahantaniaina et al., 2017). Transcriptomic analysis was performed to investigate the effect of the *mdar2* mutation on *cat2* responses in more detail, and the *cat2 dhar1 dhar2 dhar3* line was included for comparison (Fig. 5). Approximately 1500 genes were differentially expressed between Col-0 and *cat2* (Table S2). The transcriptomic signature of the *cat2* mutation was generally attenuated by the presence of additional mutations in *MDAR2* or the three *DHARs* (Fig. 5). The modulating effect of the additional mutations was particularly evident for genes that were induced in *cat2* compared to Col-0, with the clearest effects being observed in cluster 4 (Fig. 5a, C4), which was enriched in genes involved in cell death, systemic acquired resistance, SA responses, and related processes. Analysis of the expression levels of the most strongly induced genes in *cat2* revealed that loss of function of *MDAR2* or the three DHARs produced a similar dampening effect on these genes (Fig. 5b). For example, the transcription factor *WRKY31* was the most strongly compromised by the *dhar* and *mdar2* mutations. The defence-related *FMO1* and *NHL10* also showed a dampened expression in *cat2 dhar123* or *cat2 mdar2* compared to *cat2*.

Together with the data in Figure 4, this expression analysis provides evidence that a functional MDHAR2 is required to mediate some of the downstream signalling responses triggered by oxidative stress in *cat2*. To confirm this point, we sought to increase MDHAR activity in the *cat2 mdar2* line by introducing the wild-type MDHAR2 linked to GFP in C- or N-terminal. Fluorescence analyses confirmed the cytosolic localisation of MDHAR2 (Fig. 6a). Based on anti-GFP antibody tests and *MDAR2* transcript analyses, one line of each construct was selected in which *MDAR2* expression was restored to at least the level observed in *cat2* (Fig. 6b,c). In these lines, the NADH-dependent MDHAR activity was similar to or somewhat higher than in *cat2 mdar2* (Fig. 6d, left). A clearer effect was seen on the NADPH-dependent activity, which was induced in *cat2*, undetectable in *cat2 mdar2*, and restored to the *cat2* level or above in the complemented lines (Fig. 6d, right). While ascorbate contents were similar in all lines (Fig. 6e), the increased MDHAR activity in the complemented lines reversed the very high glutathione contents and oxidation state observed in *cat2 mdar2*. The restoration of *MDAR2* expression decreased glutathione accumulation and oxidation to levels comparable or below those observed in *cat2* (Fig. 6f), effects that correlated with the increased extractable NADPH-dependent MDHAR activity (Fig. 6d).

In the two complemented lines, leaf lesions were also restored to the *cat2* level (Fig.7a,b). This effect was accompanied by increased SA contents (Fig. 7c) and SA marker transcripts (Fig. 7d). We also examined three genes associated with JA signaling: although effects were less clear compared to the SA pathway, *PFD1.2* and *VSP2* were both induced in *cat2*, much less in *cat2 mdar2*, and restored in the complemented lines (Fig. 7e).

An anti-GFP pulldown strategy was implemented to identify proteins that might be part of an interacting network involving MDHAR2. For this, the strategy described in Wendrich *et al*. (2017) was used by expressing an MDAR2-GFP fusion in the *cat2 mdar2* mutant background. This analysis identified more than 100 proteins that could be grouped into different functional categories (Table S3; Fig. 8). Among potential interactants were proteins involved in regulating gene expression as well as enzymes involved in primary metabolism, including photorespiration and glycolysis (Fig. 8). These proteins included glycolytic glyceraldehyde 3-phosphate dehydrogenase, NADP-malic enzyme 2 (NADP-ME2), and isocitrate dehydrogenase (NADP-ICDH), cytosolic enzymes involved in NADH or NADPH production. Other notable groups of potential interactants included other redox-related proteins and several proteins involved in biotic stress responses (Fig. 8).

Discussion

Our aim in this study was to assess the roles of specific MDHARs in optimal and oxidative stress conditions. Observations in single *mdar* mutants grown in our conditions are consistent with a previous report, notably in showing that none of the enzymes appears to be necessary for plant growth (Tanaka et al., 2021). However, when introduced into an oxidative stress background, the importance of certain MDHARs becomes more apparent. First, loss of the peroxisomal functions somewhat exacerbated the *cat2* dwarf phenotype. This is perhaps not surprising since the major role of CAT2 is to metabolise photorespiratory H_2O_2, which is predominantly produced in the peroxisomes (Yang *et al*., 2019). It is noteworthy, however, that the *mdar1* and *mdar4* mutations were not associated with altered ascorbate or glutathione status, either in the single mutants relative to Col-0 or in the double mutants relative to *cat2*. Only the *mdar2* mutation produced a significant effect on these pools (in *cat2 mdar2*) and it was this mutation that, in removing most of the leaf lesions triggered by catalase deficiency, produced the most interesting effect: rather than exacerbating transcriptomes and phenotypes triggered by oxidative stress, loss of this secondary antioxidative function acted to oppose them. Below we discuss some of the conclusions that can be drawn from this study.

The cytosolic ascorbate-glutathione pathway is important in linking oxidative stress to phytohormone signalling

We previously reported that loss-of-function mutants for other cytosolic enzymes of the ascorbate-glutathione pathway (GR1, DHAR1, DHAR2) showed a wild-type phenotype but modulated the response to oxidative stress observed in response to catalase deficiency (Mhamdi *et al*., 2010b; Rahantaniaina *et al*., 2017). However, unequivocal conclusions on the importance of compartmentation were difficult to draw from these earlier analyses because a small part of the GR1 activity is associated with the peroxisomes (Kataya & Reumann, 2010) and it is not clear whether or not the peroxisomes contain DHAR. In the present study, we have been able to compare the importance of MDHARs located specifically in the two compartments in oxidative stress responses. Although loss of the peroxisomal *MDAR1* and *MDAR4* functions somewhat exacerbated the dwarf phenotype associated with the *cat2* mutation, it is the *mdar2* mutation that most influenced the *cat2* lesion phenotype, and this was associated with markedly decreased activation of the SA pathway. Thus, the cytosolic ascorbate-glutathione pathway appears to be a key player in transmission of oxidative stress signals that originate in other compartments. This is consistent with gene expression

patterns in *cat2*, where the cytosolic but not the peroxisomal isoforms of MDHAR were up-regulated (Fig. 2; Fig. S4).

An important role for the cytosol in governing the outcome of oxidative stress is consistent with previous reports on *apx1* mutants (Davletova *et al*., 2005; Vanderauwera *et al*., 2011). It should be noted that although CAT2 is mainly located in peroxisomes, the protein can also be located in other compartments, including the nucleus (Al-Hajaya *et al*., 2022), although the extent of ROS production in this compartment compared to the peroxisomes is unclear (Dard *et al*., 2024). It is likely that in the absence of CAT2, some H_2O_2 can move from these compartments into the cytosol, where it can be metabolised by APX, engaging downstream cytosolic enzymes such as MDHAR, DHAR, and GR (Mhamdi *et al*., 2010a). This is consistent with the observations of Ugalde et al. (2021), who reported that a cytosolic H_2O_2 probe remained more oxidized in *cat2* compared to the wild-type background after addition of H_2O_2 to young Arabidopsis seedlings.

Cytosolic MDHAR2 is the major contributor to NADPH-dependent MDHAR activity in Arabidopsis leaves

In agreement with previous data (Tanaka *et al*., 2021), our analyses suggest that peroxisomal MDHAR1 and cytosolic MDHAR2 are major isoforms in Arabidopsis leaves. MDHAR activity can be supported by either NADH or NADPH, and insight into co-factor preference is important to situate the enzymes within their metabolic context. Both total extractable leaf MDHAR and recombinant MDHAR activities are higher with NADH than NADPH. However, in addition to their differences in subcellular localization, the data show that MDHAR1 and MDHAR2 make different contributions to the activities with the two reductants (Fig. 1, Fig. 3, Table 1). The activity assays performed on recombinant proteins suggest that MDHAR1 will mainly use NADH *in vivo*, as the catalytic efficiency with NADPH is much lower. The preference of MDHAR2 is less clear. The K_m values for the two co-factors were much more similar than for MDHAR1 and well below the concentrations used in our standard assays of extractable leaf activity (250 µM). This suggests that the *mdar2* mutation should have a similar effect on the NADH- and NADPH-dependent activities measured *in vitro*, at saturating co-factor concentrations. Our data are consistent with this: in the Col-0 background, the *mdar2* mutation decreased the extractable NADPH-dependent activity by about 10 $nmol.mg^{-1}prot.min^{-1}$, which corresponds to about 50% of the total activity with this co-factor (Fig. 1b). Against the background of the much higher total activities of NADH-dependent activity, a decrease of this magnitude is harder to detect. In fact, decreases in NADH-dependent activity of this order were observed in *mdar2* but were found to be statistically insignificant against the background values,

411 which were much higher than for the NADPH-dependent activity (Fig. 1b). In the *cat2* background,
412 where *MDAR2* is induced at the transcript level and total extractable activities are increased, the
413 *mdar2* mutation affects both extractable activities, decreasing the NADPH-dependent activity by
414 about 40 nmol.mg^{-1}prot.min^{-1} and the NADH-dependent activity by a similar or greater value (Fig. 3).
415 Again, the higher total extractable activity of NADH-dependent activity makes the proportional
416 impact of the *mdar2* mutation on the NADPH-dependent activity more evident (Fig. 3).
417
418 A key point for placing these observations in their physiological context. Accurate determination of
419 reduced NAD(P) in different compartments is difficult, both from a technical and interpretative
420 viewpoint. In the cytosol, the NAD pool is substantially more oxidized than the NADP pool (Heineke
421 *et al*., 1991; Igamberdiev and Gardeström, 2003). Based on direct assays following rapid fractionation
422 of pea leaf protoplasts, cytosolic NADH was estimated to be between 18 and 55 µM (Igamberdiev
423 and Gardeström, 2003). However, these assays detected total NADH. Since a high proportion of this
424 total pool is likely to be bound to enzyme active sites at any given time, the free pool could be much
425 lower (Igamberdiev and Gardeström, 2003). Indeed, indirect estimates of cytosolic NADH
426 concentrations based on equilibrating metabolite pools produced values as low as 1 µM or less
427 (Heineke *et al*., 1991). In any case, our assays of extractable MDHAR activities at 250 µM NADH are
428 likely to be strongly over-estimating the cytosolic NADH-dependent activity *in vivo*. If so, the
429 enhanced engagement of the ascorbate-glutathione pathway in *cat2* might draw mainly on cytosolic
430 NADPH, which was estimated to be present at concentrations 3.5 to 8-fold higher than NADH in this
431 compartment (Igamberdiev and Gardeström, 2003). As well as supporting MDHAR2, the cytosolic
432 NADPH pool would be important to sustain GR activities previously shown to be important in
433 oxidative stress responses (Mhamdi *et al*., 2010b). The refinement of fluorescent probes that can
434 measure concentrations of these key cofactors *in situ* could throw further light on these issues (Smith
435 *et al*., 2022).
436
437 Observations from the GFP pulldown experiments suggest that networking with other proteins might
438 also be part of the biological functions of MDHAR2. In addition to proteins whose functional
439 connections to MDHAR2 remain to be elucidated, several enzymes were identified that are linked in
440 terms of antioxidant or other redox function. Notably, cytosolic enzymes involved in glycolysis (PGK,
441 GAPC) or NADPH production (NADP-ME2, cICDH) were identified as players within a potential
442 network that includes MDHAR2 (Fig. 8). The importance of some of these enzymes have previously
443 been examined in the *cat2* background (Mhamdi *et al*., 2010c; Li *et al*., 2013), and indeed loss of
444 *nadp-icdh* function modulates *cat2*-triggered biotic stress responses, although much less strongly
445 than the *mdar2* mutant examined in this study. Several of these NAD(P)H-generating proteins are

commonly found to be enriched proteins within other GFP pulldown experiments, possibly reflecting their abundance and importance in cytosolic metabolism (Supporting Information Table S3). Among them, NADP-ME2 has been less commonly found than the other NAD(P)H-generating systems in previous analyses, perhaps pointing to a particularly important functional association with MDHAR2. Indeed, NADP-ME2 has been implicated in pathogenesis-related responses, which was interpreted in terms of providing reductant for NADPH oxidase activity (Voll *et al*., 2012). Our data suggest that this enzyme might also influence biotic stress responses by supplying NADPH for MDHAR2.

Decreased MDHAR capacity affects glutathione but not ascorbate status during oxidative stress

It is striking that none of the mutations produced marked effects on the ascorbate pool and redox status, at least as measured globally in leaf extracts. The only significant effect was in *cat2 mdar2*, in which a modest decrease in ascorbate was sometimes but not consistently observed (Fig. 3b, Fig. 5e). Maintenance of the ascorbate pool, even when both CAT2 and MDHAR2 functions are lost, probably reflects the numerous pathways by which this molecule can be regenerated from both MDHA and DHA in plants, as well as the relatively positive redox potential of ascorbate compared to more powerful reductants such as glutathione, NAD(P)H, glutaredoxins, and thioredoxins (Foyer & Noctor, 2016).

In contrast to the stability of the ascorbate pool, a consistent and specific effect of *MDAR2* expression level and activity on glutathione was observed (Fig. 3c, Fig.6f). This is probably explainable by two effects. First, MDHAR capacity is inversely correlated with the formation of DHA, the main driver for glutathione oxidation (Rahantaniaina *et al*., 2017; Tuzet *et al*., 2019), and so decreased MDHAR activity is predicted to accelerate DHA formation, driving faster oxidation of GSH and accumulation of GSSG (Fig. 9). Second, a substantial part of the GSSG that accumulates in *cat2* is located in the vacuole, where it is protected from immediate re-reduction, making glutathione a more informative marker of sustained oxidative stress than ascorbate (Queval *et al*., 2011).

Possible mechanisms to explain the influence of MDHAR2

While other pathways exist in plants, catalase and the ascorbate-glutathione pathway can be considered as important H_2O_2-processing systems acting in parallel. Given this, perhaps the most striking of our observations is that loss of cytosolic *MDAR2* function does not exacerbate *cat2* phenotypes but instead partly reverts them. This is not the first observation of this kind. In both

tobacco and Arabidopsis, decreasing APX and catalase expression produced phenotypes that were less severe than in plants lacking only one of the enzymes (Rizshsky et al., 2002; Vanderauwera et al., 2011). While differences in experimental protocols and growth regimes make it difficult to compare our studies with these previous ones, some of the mechanisms could be partly shared. In Arabidopsis lines doubly deficient in catalase and APX, an ameliorated phenotype was associated with induction of a DNA repair pathway that was not activated in plants lacking only one of the enzymes (Vanderauwera et al., 2011). Hence, we queried our transcriptomics data for the response of genes involved in such DNA repair pathways. However, they provide little evidence that this can explain the effect of *mdar2* on *cat2*-triggered responses in the growth conditions of moderate irradiance we have used here.

What is the nature of the MDHAR-related signal that seems to be important to link oxidative stress to downstream signalling? One possibility is that the MDHAR2 protein acts as a sensor of H_2O_2 or oxidative stress signals, although we do not have any direct evidence for such a role. Indirect effects in signalling cannot be ruled out. For example, some cytosolic peroxiredoxins are induced alongside APX1 and cytosolic MDARs in *cat2* (Supplemental Figure S4). Through intermediate GRX activity, these peroxiredoxins can oxidize glutathione (Bréhélin *et al*., 2003), an influential player in pathogenesis-related responses (Noctor *et al*., 2024). However, whether glutathione oxidation occurs solely as shown in Figure 9 or additionally through other pathways, our data provide little evidence for a simple role of glutathione status in linking oxidative stress and induction of the SA pathway. This is because the *dhar* and *mdar* mutations produced strikingly overlapping effects on pathways related to biotic stress (Fig. 5), whereas they have opposite effects on glutathione; ie, *dhar* mutations antagonize both *cat2*-triggered glutathione oxidation and SA accumulation (Rahantaniana *et al*., 2017) while the *mdar2* mutation antagonizes SA accumulation but promotes glutathione oxidation (Figs 3, 4 and 6). We cannot exclude the possibility that altered glutathione status affects the GSNO/GSNO reductase system, which plays a role in oxidative stress responses in *cat2* (Zhang *et al*., 2020). MDHAR2 might also act to catalyse ROS production in a secondary reaction, in a similar way to the mitochondrial MDHAR5, which promotes sensitivity to certain xenobiotics in this way (Johnston *et al*., 2015). Based on available knowledge, this could require a sensitizing redox-cycling metabolite, with which MDHAR2 would interact, to accumulate during oxidative stress. In this connection, it should be noted that we have previously used different techniques to attempt to quantify ROS, including H_2O_2, in *cat2* and derived lines. However, signals were consistently found to be variable and not greatly different from the wild-type, even under conditions in which *cat2* plants are clearly undergoing oxidative stress (Queval *et al*., 2008; Mhamdi *et al*., 2010b; Yang *et al*., 2019). Similarly, we have invested considerable effort in developing mutant lines that express roGFP and related

probes, but gene silencing in mutant backgrounds and the difficulty of measuring signals in the mesophyll cells of mature leaves have prevented progress with these measurements.

Finally, given the similarity of the effects of the *mdar2* and *dhar* mutations on oxidative stress-triggered responses (Fig. 5), one other hypothesis is that accumulation of oxidized forms of ascorbate in the cytosol might interlink with key regulators in phytohormone or other signalling pathways. Ascorbate-deficient mutants show some spontaneous activation of SA-related pathogenesis-related pathways (Pastori *et al*., 2003; Pavet *et al*., 2005) and attention has been drawn to the potential importance of ascorbate oxidase (which produces MDHA) in influencing defence and phytohormone signalling (Pignocci *et al*., 2006). Such observations are often interpreted in terms of the roles of ascorbate as a redox buffer or indirect effects on ROS contents. However, plants with decreased ascorbate might be expected to have lower MDHA and DHA (by adjustment of the equilibrium between ascorbate, DHA, and MDHA). Similarly, loss of DHAR function might also boost MDHA concentrations as a secondary effect. If either of the two oxidized forms of ascorbate is capable of binding to signal transduction proteins to interfere with biotic stress responses, such interactions might explain some of our observations in this work and those previously reported in other plants with alterations in ascorbate contents or metabolism. While this notion remains hypothetical, such effects would add greater subtlety to the influence of the ascorbate-glutathione pathway on cellular function: cell signalling could be impacted not only by the capacity of the pathway to remove ROS themselves but also by ROS-mediated effects on the concentrations of pathway intermediates.

Acknowledgments

Dongdong Xu and Zheng Yang were supported by PhD grants from the China Scholarship Council. Lug Trémulot is supported by a PhD grant from the Université Paris Saclay and MESRI (Ministère de l'Enseignement Supérieur, de la Recherche, et de l'Innovation), France. The GN laboratory received financial support from the French Agence Nationale de la Recherche HIPATH project (ANR-17-CE20-0025) and the Institut Universitaire de France (IUF). The FVB laboratory is supported in part by the Research Foundation Flanders (FWO) (The Excellence of Science [EOS] Research project 869 30829584), and NUCLEOX (grant number G007723N). We are grateful to Ivan Couée (Université de Rennes, France) for stimulating discussions.

Author contributions

D.X., Z.Y., G.C-I. produced, characterized and analysed the mutants and transgenic lines. D.X., C.E., and E.I-B. produced the recombinant proteins. L.T., A.M., L.M. and F.V.B. contributed analysis of transcriptomics and proteomics data. H.V., E.I-B., and GN conceived the project, supervised experimental work, and interpreted data. Together with input from co-authors, G.N. wrote the manuscript.

Supplemental Data

Supporting Information Figure S1. Gene maps and genotyping of *mdar* mutants.

Supporting Information Figure S2. Photographs of *mdar* mutants and rosette fresh weights

Supporting Information Figure S3. Kinetic curves for MDHAR activity of recombinant proteins.

Supporting Information Figure S4. Effect of the *cat2* mutation on expression of some of the major H_2O_2-metabolizing pathways in Arabidopsis.

Supporting Information Figure S5. Analysis of expression of *MDAR* genes in the *cat2* background.

Supporting Information Table S1. List of gene primers.

Supporting Information Table S2. List of differentially expressed genes in the different mutants.

Supporting Information Table S3. List of potential MDHAR2 interactants.

References

Al-Hajaya, Karpinska B, Foyer CH, Baker A. 2022. Nuclear and peroxisomal targeting of catalase. *Plant, Cell & Environment* **45:** 1096–1108.

Aliverti A, Curti B, Vanoni MA. 1999. Identifying and quantitating FAD and FMN in simple and in iron-sulfur-containing flavoproteins. *Methods in Molecular Biology* **131:** 9-23.

Bérczi A, Møller IM. 1998. NADH-monodehydroascorbate oxidoreductase is one of the redox enzymes in spinach leaf plasma membranes. *Plant Physiology* **116:** 1029–1036.

Bohrer AS, Massot V, Innocenti G, Reichheld JP, Issakidis-Bourguet E, Vanacker H. 2012. New insights into the reduction systems of plastidial thioredoxins point out the unique properties of thioredoxin z from Arabidopsis. *Journal of Experimental Botany* **63:** 6315-6323.

Bréhélin C, Meyer EH, de Souris J-P, Bonnard G, Meyer Y. 2003. Resemblance and dissemblance of Arabidopsis Type II peroxiredoxins: similar sequences for divergent gene expression, protein localization, and activity. *Plant Physiology* **132,** 2045-2057.

Chaouch S, Queval G, Vanderauwera S, Mhamdi A, Vandorpe M, Langlois-Meurinne M, Van Breusegem F, Saindrenan P, Noctor G. 2010. Peroxisomal H_2O_2 is coupled to biotic defense responses by ICS1 in a daylength-dependent manner. *Plant Physiology* **153:** 1692-1705.

Cheng CY, Krishnakumar V, Chan AP, Thibaud-Nissen F, Schobel S, Town CD. 2017. Araport11: a complete reannotation of the Arabidopsis thaliana reference genome. *The Plant Journal* **89:** 789-804.

Chew O, Whelan J, Millar AH. 2003. Molecular definition of the ascorbate-glutathione cycle in Arabidopsis mitochondria reveals dual targeting of antioxidant defenses in plants. *Journal of Biological Chemistry* **278:** 46869-46877.

Clough SJ, Bent AF. 1998. Floral dip: A simplified method for *Agrobacterium*-mediated transformation of *Arabidopsis thaliana*. *The Plant Journal* **16:** 735–743.

Conklin PL, Foyer CH, Hancock RD, Ishikawa T, Smirnoff N. 2024. Ascorbate acid metabolism and functions. *Journal of Experimental Botany* **75:** 2599-2603.

Dard A, Van Breusegem F, Mhamdi A. 2024. Redox regulation of gene expression: proteomics reveals multiple previously undescribed redox-sensitive cysteines in transcription complexes and chromatin modifiers. *Journal of Experimental Botany* 75, XXXX-XXXX

Davletova S, Rizhsky L, Liang H, Shengqiang Z, Oliver DJ, Coutu J, Shulaev V, Schlauch K, Mittler R. 2005. Cytosolic ascorbate peroxidase 1 is a central component of the reactive oxygen gene network of Arabidopsis. *The Plant Cell* **17:** 268-281.

Dobin A, Davis CA, Schlesinger F, Drenkow J, Zaleski C, Jha S, Batut P, Chaisson M, Gingeras TR. 2013. STAR: ultrafast universal RNA-seq aligner. *Bioinformatics* **29:** 15-21.

Dowdle J, Ishikawa T, Gatzek S, Rolinski S, Smirnoff N. 2007. Two genes in Arabidopsis thaliana encoding GDP-l- galactose phosphorylase are required for ascorbate bio- synthesis and seedling viability. *The Plant Journal* **52:** 673–689.

Eastmond PJ. 2007. MONODEHYDROASCORBATE REDUCTASE4 is required for seed storage oil hydrolysis and postgerminative growth in Arabidopsis. *The Plant Cell* **19:** 1376–1387.

El Airaj H, Gest N, Truffault V, Garchery C, Riqueau G, Gouble B, Page D, Stevens R. 2013. Decreased monodehydroascorbate reductase activity reduces tolerance to cold storage in tomato and affects fruit antioxidant levels. *Postharvest Biology and Technology* **86:** 502-510.

Foyer CH, Halliwell B. 1977. Purification and properties of dehydroascorbate reductase from spinach leaves. *Phytochemistry* **16:** 1347-1350.

Foyer CH, Kunert K. **2024.** The ascorbate–glutathione cycle coming of age. *Journal of Experimental Botany* **75:** 2682-2699.

Foyer CH, Noctor G. 2016. Stress-triggered redox signalling: What's in pROSpect? *Plant, Cell & Environment* **39:** 951-964.

Gest N, Garchery C, Gautier H, Jimenez A, Stevens R. 2013. Light-dependent regulation of ascorbate in tomato by a monodehydroascorbate reductase localized in peroxisomes and the cytosol. *Plant Biotechnology Journal* **11:** 344–354.

Gradogna A, Lagostena L, Beltrami S, Tosato E, Picco C, Scholz-Starke J, Sparla F, Trost P, Caraneto A. 2023. Tonoplast cytochrome *b*561 is a transmembrane ascorbate-dependent monodehydroascorbate reductase: functional characterization of electron currents in plant vacuoles. *New Phytologist* **238:** 1957-1971.

Gu Z, Eils R, Schlesner M. 2016. Complex heatmaps reveal patterns and correlations in multidimensional genomic data. *Bioinformatics* **32:** 2847-2849.

Hamada A, Tanaka Y, Ishikawa T, Maruta T. 2023. Chloroplast dehydroascorbate reductase and glutathione cooperatively determine the capacity for ascorbate accumulation under photooxidative stress conditions. *The Plant Journal* **114:** 68-82.

He H, Denecker J, Van Der Kelen K, Willems P, Pottie R, Phua SY, Hannah MA, Vertommen D, Van Breusegem F, Mhamdi A. 2021. The Arabidopsis mediator complex subunit 8 regulates oxidative stress responses. *The Plant Cell* **33:** 2032-2057.

Heineke D, Riens B, Grosse H, Hoferichter P, Peter U, Flügge U-I, Heldt HW. 1991. Redox transfer across the inner chloroplast envelope membrane. *Plant Physiology* **95:** 1131-1137.

Höfgen R, Willmitzer L. 1988. Storage of competent cells for *Agrobacterium* transformation. *Nucleic Acids Research* **16:** 9877.

Hooper CM, Castleden I, Tanz SK, Grasso SV, Aryamanesh N, and Millar AH. 2022. Subcellular Localisation database for Arabidopsis proteins version 5.

Hossain MA, Asada K. 1984. Purification of dehydroascorbate reductase from spinach and its characterisation as a thiol enzyme. *Plant Cell Physiology* **25:** 85-92.

Hossain MA, Asada K. 1985. Monodehydroascorbate reductase from cucumber is a flavin adenine dinucleotide enzyme. *Journal of Biological Chemistry* **260:** 12920-12926.

Hossain MA, Nakano Y, Asada K. 1984. Monodehydroascorbate reductase in spinach chloroplasts and its participation in regeneration of ascorbate for scavenging hydrogen peroxide. *Plant Cell Physiology* **25:** 385-395.

Koncz C, Schell J. 1986. The promoter of Ti-DNA gene 5 controls the tissue-specific expression of chimeric genes carried by a novel type of Agrobacterium binary vector. *Molecular and General Genetics* **204:** 383–396

Igamberdiev AU, Gardeström P. 2003. Regulation of NAD- and NADP-dependent isocitrate dehydrogenases by reduction levels of pyridine nucleotides in mitochondria and cytosol of pea leaves. *Biochimica et Biophysica Acta* **1606:** 117–125

Johnston EJ, Rylott EL, Beynon E, Lorenz A, Chechik V, Bruce NC. 2015. Monodehydroascorbate reductase mediates TNT toxicity in plants. *Science* **349:** 1071-1075.

Kataya AMR, Reumann S. 2010. Arabidopsis glutathione reductase 1 is dually targeted to peroxisomes and the cytosol. *Plant Signaling and Behaviour* **5:** 171–175.

Karimi M, Inzé D, Depicker A. 2002. GATEWAY vectors for Agrobacterium- mediated plant transformation. *Trends in Plant Science* **7:** 193–195.

Lambert I, Paysant-Le Roux C, Colella S, Martin-Magniette ML. 2020. DiCoExpress: a tool to process multifactorial RNAseq experiments from quality controls to co-expression analysis through differential analysis based on contrasts inside GLM models. Plant Methods **16:** 68.

Li S, Mhamdi A, Clement C, Jolivet Y, Noctor G. 2013. Analysis of knockout mutants suggests that Arabidopsis NADP-MALIC ENZYME2 does not play an essential role in responses to oxidative stress of intracellular or extracellular origin. *Journal of Experimental Botany* **64:** 3605-3614.

Liao Y, Smyth GK, Shi W. 2014. featureCounts: an efficient general purpose program for assigning sequence reads to genomic features. *Bioinformatics* **30:** 923-930.

Lisenbee CS, Lingard MJ, Trelease RN. 2005. Arabidopsis peroxisomes possess functionally redundant membrane and matrix isoforms of monodehydroascorbate reductase. *The Plant Journal* **43:** 900-914.

Maynard D, Kumar V, Sproß J, Dietz K-J. 2020. 12-Oxophytodienoic acid reductase 3 (OPR3) functions as NADPH-dependent α,β-ketoalkene reductase in detoxification and monodehydroascorbate reductase in redox homeostasis. *Plant & Cell Physiology* **61:** 584–595.

Mhamdi A, Queval G, Chaouch S, Vanderauwera S, Van Breusegem F, Noctor G. 2010a. Catalases in plants: a focus on Arabidopsis mutants as stress-mimic models. *Journal of Experimental Botany* **61:** 4197-4220.

Mhamdi A, Hager J, Chaouch S, Queval G, Han Y, Taconnat Y, Saindrenan P, Issakidis-Bourguet E, Gouia H, Renou JP, Noctor G. 2010b. Arabidopsis GLUTATHIONE REDUCTASE 1 is essential for the metabolism of intracellular H_2O_2 and to enable appropriate gene expression through both salicylic acid and jasmonic acid signaling pathways. *Plant Physiology* **153:** 1144-1160.

Mhamdi A, Mauve C, Gouia H, Saindrenan P, Hodges M, Noctor G. 2010c. Cytosolic NADP-dependent isocitrate dehydrogenase contributes to redox homeostasis and the regulation of pathogen responses in Arabidopsis leaves. *Plant, Cell & Environment* **33:** 1112-1123.

Miyake C, Asada K. 1994. Ferredoxin-dependent photoreduction of the monodehydroascorbate radical in spinach thylakoids. *Plant Cell Physiology* **35:** 539-549.

Noctor G. 2015. Lighting the fuse on toxic TNT. *Science* **349:** 1052-1053.

Noctor G, Mhamdi A. 2022. Quantitative measurement of ascorbate and glutathione by spectrophotometry. In Methods in Molecular Biology. Reactive Oxygen Species in Plants: methods and protocols (A Mhamdi, ed), pp. 87-96. Humana, New York, NY.

Noctor G, Mhamdi A, Foyer CH. 2016. Oxidative stress and antioxidative systems: recipes for successful data collection and interpretation. *Plant, Cell & Environment* **39:** 1140–1160.

Noctor G, Cohen MC, Trémulot L, Châtel-Innocenti G, Van Breusegem F, Mhamdi A. 2024. Glutathione: a key modulator of plant defence and metabolism through multiple mechanisms. *Journal of Experimental Botany* **75:** 4549-4572.

Noshi M, Yamada H, Hatanaka R, Tanabe N, Tamoi M, Shigeoka S. 2017. Arabidopsis dehydroascorbate reductase 1 and 2 modulate redox states of ascorbate-glutathione cycle in the cytosol in response to photooxidative stress. *Bioscience Biotechnology & Biochemistry* **81:** 523–533.

Pasha A, Subramaniam S, Cleary A, Chen X, Berardini T, Farmer A, Town C, Provart N. 2020. Araport lives: an updated framework for Arabidopsis bioinformatics. *The Plant Cell* **32:** 2683-2686.

Pastori GM, Kiddle G, Antoniw J, Bernard S, Veljovic-Jovanovic S, Verrier PJ, Noctor G, Foyer CH. 2003. Leaf vitamin C contents modulate plant defense transcripts and regulate genes that control development through hormone signalling. *The Plant Cell* **15:** 939-951.

Pavet V, Olmos E, Kiddle G, Mowla S, Kumar S, Antoniw J, Alvarez ME, Foyer CH. 2005. Ascorbic acid deficiency activates cell death and disease resistance responses in Arabidopsis. *Plant Physiology* **139:** 1291-1303.

Pignocci C, Kiddle G, Hernández I, Foster SJ, Asensi A, Taybi T, Barnes J, Foyer CH. 2006. Ascorbate oxidase-dependent changes in the redox state of the apoplast modulate gene transcript

accumulation leading to modified hormone signaling and orchestration of defense processes in tobacco. *Plant Physiology* **141:** 423-435.

Queval G, Noctor G. 2007. A plate reader method for the measurement of NAD, NADP, glutathione, and ascorbate in tissue extracts: application to redox profiling during Arabidopsis rosette development. *Analytical Biochemistry* **363:** 58–69.

Queval G, Hager J, Gakière B, Noctor G. 2008. Why are literature data for H_2O_2 contents so variable? A discussion of potential difficulties in quantitative assays of leaf extracts. *Journal of Experimental Botany* **59:** 135-146.

Queval G, Thominet D, Vanacker H, Miginiac-Maslow M, Gakière B, Noctor G. 2009. H_2O_2-activated up-regulation of glutathione in Arabidopsis involves induction of genes encoding enzymes involved in cysteine synthesis in the chloroplast. *Molecular Plant* **2:** 344–356.

Queval G, Jaillard D, Zechmann B, Noctor G. 2011. Increased intracellular H_2O_2 availability preferentially drives glutathione accumulation in vacuoles and chloroplasts. *Plant, Cell & Environment* **34:** 21-32.

Rahantaniana MS, Li S, Chatel-Innocenti G, Tuzet A, Issakidis-Bourguet E, Mhamdi A, Noctor G. 2017. Cytosolic and chloroplastic DHARs cooperate in the induction of the salicylic acid pathway by oxidative stress. *Plant Physiology* **174:** 956-971.

Rizhsky L, Hallak-Herr E, Van Breusegem F, Rachmilevitch S, Barr JE, Rodermel S, Inzé D, Mittler R. 2002. Double antisense plants lacking ascorbate peroxidase and catalase are less sensitive to oxidative stress than single antisense plants lacking ascorbate peroxidase or catalase. *The Plant Journal* **32:** 329-342.

Sano S, Miyake C, Mikami B, Asada K. 1995. Molecular characterization of monodehydroascorbate radical reductase from cucumber highly expressed in *Escherichia coli*. *Journal of Biological Chemistry* **270:** 21354–2136.

Shannon P, Markiel A, Ozier O, Baliga NS, Wang JT, Ramage D, Amin N, Schwikowski B, Ideker T. 2003. Cytoscape: a software environment for integrated models of biomolecular interaction networks. *Genome Research* **13:** 2498-2504.

Schippers JHM, von Bongartz K, Laritzki L, Frohn S, Frings S, Renziehausen T, Augstein F, Winkels K, Sprangers K, Sasidharan R, Vertommen D, Van Breusegem F, Hartman S, Beemster GTS, Mhamdi A, van Dongen JT, Schmidt-Schippers RR. 2024. ERFVII-controlled hypoxia responses are in part facilitated by MEDIATOR SUBUNIT 25 in *Arabidopsis thaliana*. *The Plant Journal* doi: 10.1111/tpj.17018.

Smith EN, Schwarzländer M, Ratcliffe RG, Kruger N. 2022. Shining a light on NAD- and NADP-based metabolism in plants. *Trends in Plant Science* **28:** 1072-1086.

Tanaka M, Takahashi R, Hamada A, Terai Y, Ogawa T, Sawa Y, Ishikawa T, Maruta T. 2021. Distribution and functions of monodehydroascorbate reductases in plants: comprehensive reverse genetic analysis of *Arabidopsis thaliana* enzymes. *Antioxidants* **10:** 1726.

Terai Y, Ueno H, Ogawa T, Sawa Y, Miyagi A, Kawai-Yamada M, Ishikawa T, Maruta T. 2020. Dehydroascorbate reductases and glutathione set a threshold for high-light–induced ascorbate accumulation. *Plant Physiology* **183:** 112-122.

Tuzet A, Rahantaniaina MS, Noctor G. 2019. Analyzing the function of catalase and the ascorbate-glutathione pathway in H_2O_2 processing: insights from an experimentally constrained kinetic model. *Antioxidants & Redox Signaling* **30:** 1238-1268.

Ugalde JM, Fuchs P, Nietzel T, Cutolo EA, Homagk M, Vothknecht UC, Holuigue L, Schwarzländer M, Müller-Schüssele SJ, Meyer AJ. 2021. Chloroplast-derived photo-oxidative stress causes changes in H_2O_2 and E_{GSH} in other subcellular compartments. *Plant Physiology* **186:** 125-141.

Wendrich JR, Boeren S, Möller BK, Weijers D, De Rybel B. 2017. In vivo identification of plant protein complexes using IP-MS/MS. In: Kleine-Vehn, J., Sauer, M. (eds) Plant Hormones. *Methods in Molecular Biology* **1497:** 147-158. Humana Press, New York, NY.

Vanacker H, Guichard M, Bohrer AS, Issakidis-Bourguet E. 2018. Redox regulation of monodehydroascorbate reductase by thioredoxin y in plastids revealed in the context of water stress. *Antioxidants* **7:** 183.

Vanderauwera S, Suzuki N, Miller G, van de Cotte B, Morsa S, Ravanat JL, Hegie A, Triantaphylidès C, Shulaev V, Van Montagu MC, Van Breusegem F, Mittler R. 2011. Extranuclear protection of chromosomal DNA from oxidative stress. *Proceedings of the National Academy of Sciences, USA* **108:** 1711–1716.

Veljovic-Jovanovic S, Oniki T, Takahama U. 1998. Detection of monodehydroascorbic acid radical in sulfite-treated leaves and mechanism of its formation. *Plant Cell Physiology* **39:** 1203-1208.

Voll LM, Zell MB, Engelsdorf T, Saur A, Wheeler MG, Drincovich MF, Weber APM, Maurino VG. 2012. Loss of cytosolic NADP-malic enzyme 2 in *Arabidopsis thaliana* is associated with enhanced susceptibility to *Colletotrichum higginsianum. New Phytologist* **195:** 189-202.

Xu S, Hu E, Cai Y, Xie Z, Luo X, Zhan L, Tang W, Wang Q, Liu B, Wang R, Xie W, Wu T, Xie L, Yu G. 2024. Using clusterProfiler to characterize multiomics data. *Nature Protocols* ISSN 1750-2799, doi:10.1038/s41596-024-01020-z

Yang Z, Mhamdi A, Noctor G. 2019. Analysis of catalase mutants underscores the essential role of CATALASE2 for plant growth and day length-dependent oxidative signalling. *Plant, Cell & Environment* **42:** 688-700.

Zhang T, Ma M, Chen T, Zhang L, Fan L, Zhang W, Wei B, Zhang D, Li S, Xuan W, Noctor G, Han Y. 2020. Arabidopsis S-NITROSOGLUTATHIONE REDUCTASE1 coordinates glutathione-mediated

activation of the salicylic acid pathway in response to intracellular oxidative stress. *Plant, Cell & Environment* **43:** 1175-1191.

Figure legends

Figure 1. Effects of specific *mdar* mutations on expression, extractable activities, and contents of ascorbate and glutathione. a. qRT-PCR analysis of *MDAR* expression in the different lines, normalised to *ACTIN2* and *PP2A* as reference genes. b. Effects of mutations on NADH and NADPH-dependent activities. c. Ascorbate contents. d. Glutathione contents. For c and d, numbers above the columns indicate percentage reduced (100 x reduced form/total content). Data are means ± SE of three biological replicates from different plants. Student's t-test, * Indicates significant differences compared to Col-0 at $P < 0.05$. FW: fresh weight. White bars: ASC or GSH, black bars: DHA or GSSG.

Figure 2. Response of *MDAR* expression and MDHAR activities to intracellular oxidative stress in *cat2*. a. Transcripts measured by qRT-PCR. Data were quantified relative to *ACTIN2* and *PP2A* as reference genes, and then normalised to the Col-0 value. b. NADH- and NADPH-dependent MDHAR activities. Data are means ± SE of three biological replicates from different plants. Student's t-test, * Indicates significant difference compared to Col-0 at $P < 0.05$.

Figure 3. Effects of *mdar* mutations on MDHAR activities and contents of ascorbate and glutathione in the *cat2* background. a. NADH- and NADPH-dependent MDHAR activities. b. Ascorbate contents. c. Glutathione contents. Data are means ± SE of three biological replicates from different plants. *Significant difference compared to Col-0 at $P < 0.05$; $^{+}$significant differences between double mutants and *cat2* at $P < 0.05$. Numbers above the columns indicate percentage reduced (100 x reduced form/total content). For b and c, white bars: ASC or GSH, black bars: DHA or GSSG. ^{a}Significant differences in reduced forms between double mutants and *cat2* at $P < 0.05$. ^{b}Significant differences in oxidized forms between double mutant and *cat2* at $P < 0.05$.

Figure 4. Effect of *mdar* mutations on the *cat2* phenotype and the SA pathway. a. Photographs of rosettes. b. Fresh weight and lesion quantification. Data are means ± SE of the values for 10 individual plants. c. SA contents. d. *PR* gene expression. Data are means ± SE of three biological replicates from different plants. Student's t-test, *Significant difference compared to Col-0 at $P < 0.05$. $^{+}$Significant differences of double mutants compared with *cat2* at $P < 0.05$. Bars = 1 cm. ND: not detected.

Figure 5. Transcriptomic analysis of *cat2*, *cat2 mdar2*, and *cat2 dhar1 dhar2 dhar3*. a. Heatmap showing normalized expression (Z-score of CPM) of the 1521 differentially expressed genes between Col-0 and *cat2* (FDR<0.01 & $|\log_2 FC|>1$). The top 10 of Biological Process GO enrichment for each of

the 4 clusters is displayed on the right (p-adjust<0.05). The circle size corresponds to the number of DEGs responsible for the enrichment. A joining line indicates a link between GO terms.
b. Effects of secondary mutations in ascorbate regeneration on the 20 genes with the highest fold change for *cat2* compared to Col-0. The fold change is calculated using mean CPM and Col-0 as reference.

Figure 6. Complementation of *cat2 mdar2* with GFP-MDAR2. a. GFP analysis of subcellular localisation of MDHAR2. The bar indicates 10 µm. b. Verification of *MDAR2* expression in the complemented lines using an anti-GFP antibody. c. Verification of complemented *MDAR2* transcripts. d. Effects on MDHAR activities. e. Effects on ascorbate contents. Numbers above the bars indicate % reduction. f. Effects on glutathione contents. Numbers above the bars indicate % reduction. Data are means ± SE of three biological replicates from different plants. *Significant difference compared to *cat2* at $P < 0.05$. $^{+}$Significant differences of complemented lines compared with *cat2 mdar2* at $P < 0.05$. For c and d, the white columns represent untransformed lines, the grey column represents the C-terminal transformed line, and the black column represents the N-terminal transformed line. ND: not detected. In e and f, ^{b} indicates significant differences of oxidized forms in the double mutant compared with *cat2* at $P < 0.05$ and ^{c} indicates significant differences in oxidized forms of MDAR2 complemented lines compared with *cat2 mdar2* at $P < 0.05$.

Figure 7. Complementation of *cat2 mdar2* with GFP-MDAR2 restores the *cat2* lesion phenotype and pathogenesis-related pathways. a. Phenotypes of complemented lines. b. Leaf lesion area quantification. c. SA contents. d. SA-related gene expression. e. JA-related gene expression. The white columns represent untransformed lines, the grey column represents the C-terminal transformed line, and the black column represents the N-terminal transformed line. *Significant difference compared to *cat2* at $P < 0.05$. $^{+}$Significant differences of complemented lines compared with *cat2 mdar2* at $P < 0.05$.

Figure 8. Overview of immunoprecipitation–mass spectrometry (IP-MS) search for protein interactants in *cat2 mdar2* MDAR2-GFP. The interactants shown have an enrichment ratio >25 and a p-value < 0.05. Proteins are grouped by biological processes. The box colour corresponds to the $\log_2$(enrichment ratio) with MDAR2 protein. For more details on proteins, see Supporting Information Table S3.

Figure 9. Impact of oxidative stress and MDHAR capacity on measured glutathione status. In conditions where H_2O_2 can be largely removed by catalase (a), flux through the ascorbate and

glutathione pools is low and glutathione remains highly reduced. When catalase is decreased (b), flux through the ascorbate pool is increased, causing accelerated formation of both MDHA and DHA, with the latter engaging the glutathione pool, leading to GSSG accumulation. When flux is high and MDHAR is decreased (c), conversion of MDHA to DHA is increased compared to b and the glutathione pool is further engaged, leading to even higher GSSG accumulation. Note that the pathway is shown in simplified form and that reactions are not shown stoichiometrically.

Table 1. Kinetic constants for recombinant MDHAR1 and MDHAR2 with NADH or NADPH as co-factor.

	MDHAR1		MDHAR2	
	NADH	NADPH	NADH	NADPH
V_{max} (µmol.min^{-1}mg^{-1} prot)	3426 ± 82	1119 ± 59	2074 ± 211	906 ± 45
K_m (µM)	8.23 ± 0.71	217 ± 18	3.5 ± 0.34	9.49 ± 0.2
Specific activity (V_{max}/K_m)	684	4	593	96

Data and standard errors are means of values obtained with three different curves (Fig. S4). Similar results were obtained with different protein preparations.

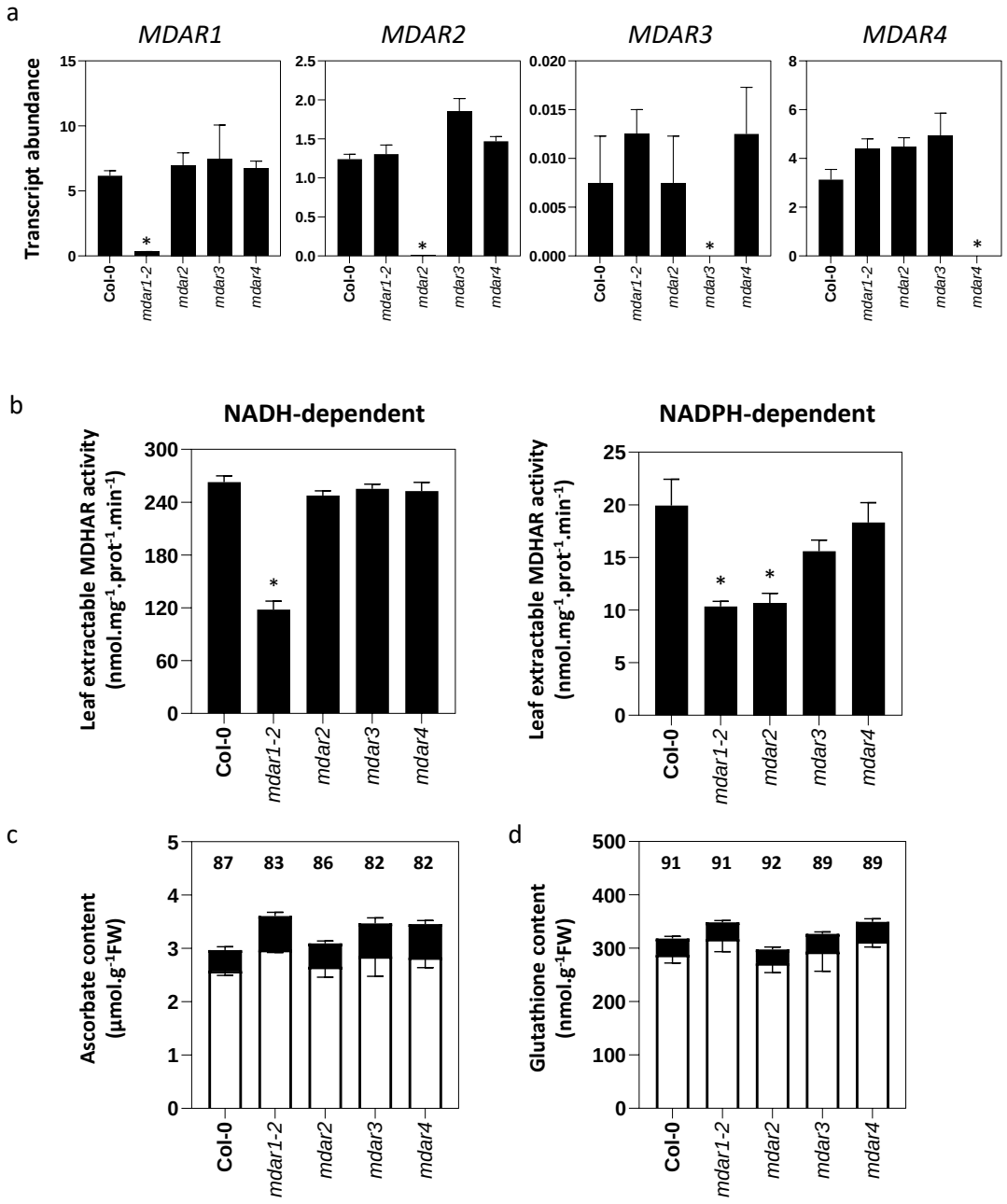

Figure 1. Effects of specific *mdar* mutations on expression, extractable activities, and contents of ascorbate and glutathione. a. qRT-PCR analysis of *MDAR* expression in the different lines, normalised to *ACTIN2* and *PP2A* as reference genes. b. Effects of mutations on NADH and NADPH-dependent activities. c. Ascorbate contents. d. Glutathione contents. For c and d, Numbers above the columns indicate percentage reduced (100 x reduced form/total content). Data are means ± SE of three biological replicates. Student's t-test, * Indicates significant differences compared to Col-0 at $P < 0.05$. FW: fresh weight. White bars: ASC or GSH, black bars: DHA or GSSG.

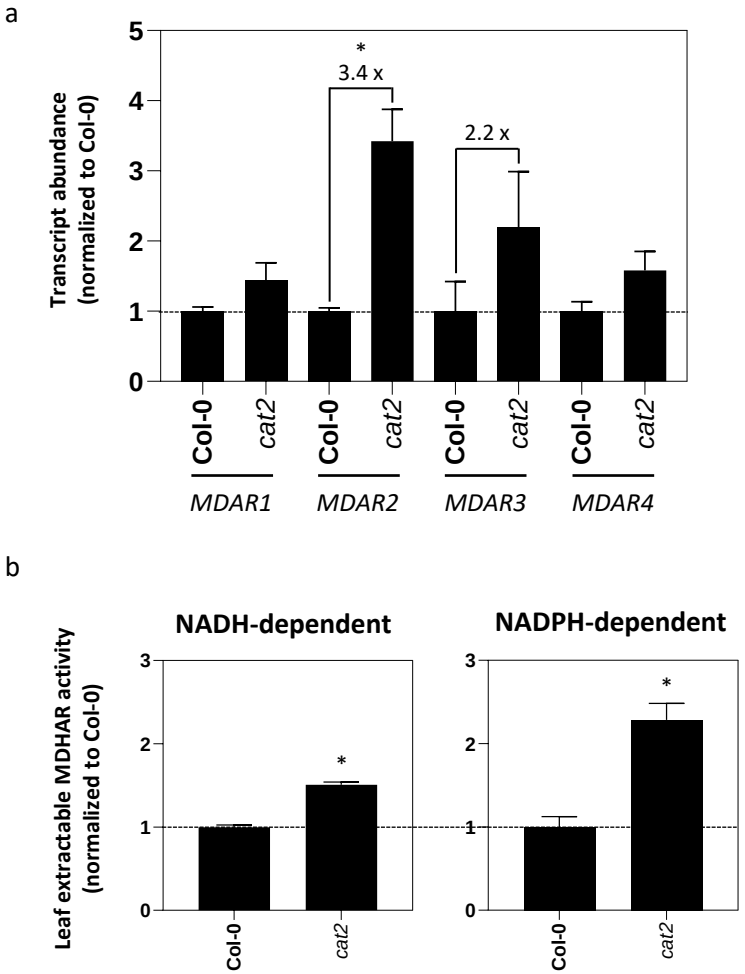

Figure 2. Response of *MDAR* expression and MDHAR activities to intracellular oxidative stress in *cat2*. a. Transcripts measured by qRT-PCR. Data were quantified relative to *ACTIN2* and *PP2A* as reference genes, and then normalised to the Col-0 value. b. NADH- and NADPH-dependent MDHAR activities. Data are means ± SE of three biological replicates. Student's t-test, * Indicates significant difference compared to Col-0 at $P < 0.05$.

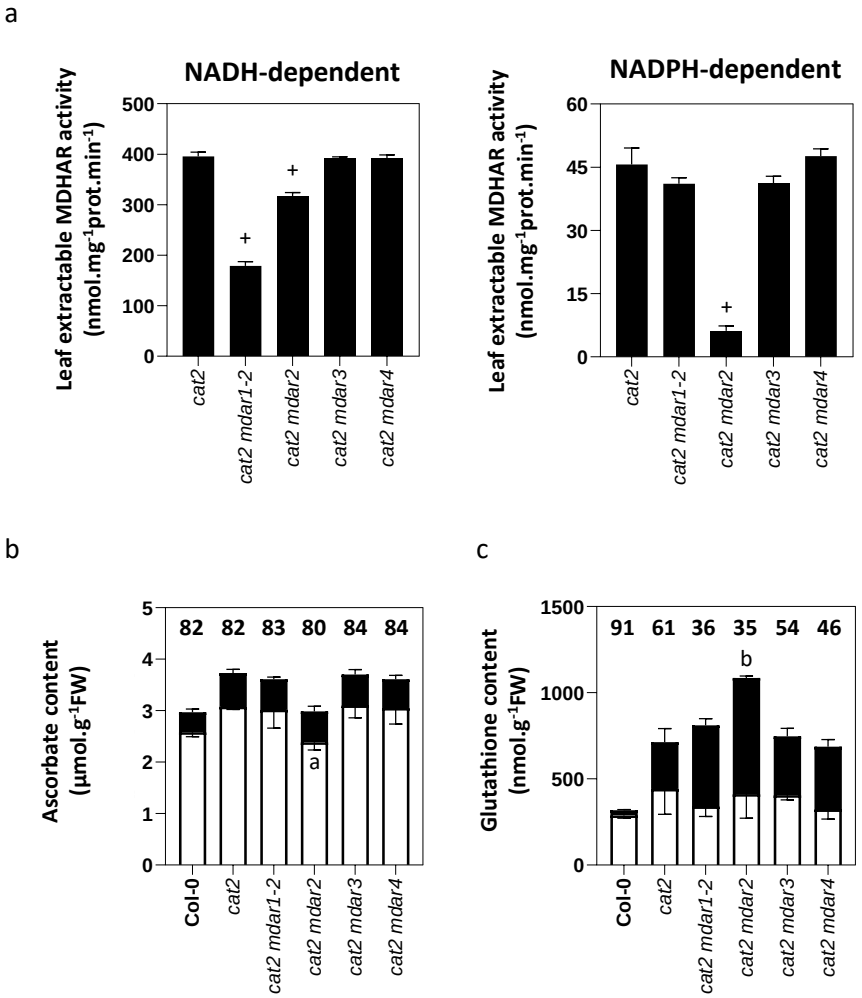

Figure 3. Effects of *mdar* mutations on MDHAR activities and contents of ascorbate and glutathione in the *cat2* background. a. NADH- and NADPH-dependent MDHAR activities. b. Ascorbate contents. c. Glutathione contents. Data are means ± SE of three biological replicates. * indicates significant difference compared to Col-0 at $P < 0.05$; + indicates significant differences between double mutants and *cat2* at $P < 0.05$. Numbers above the columns indicate percentage reduced (100 x reduced form/total content). For b and c, White bars: ASC or GSH, black bars: DHA or GSSG. [a]Significant differences in reduced forms between double mutants and *cat2* at $P < 0.05$. [b]Significant differences in oxidized forms between double mutant and *cat2* at $P < 0.05$.

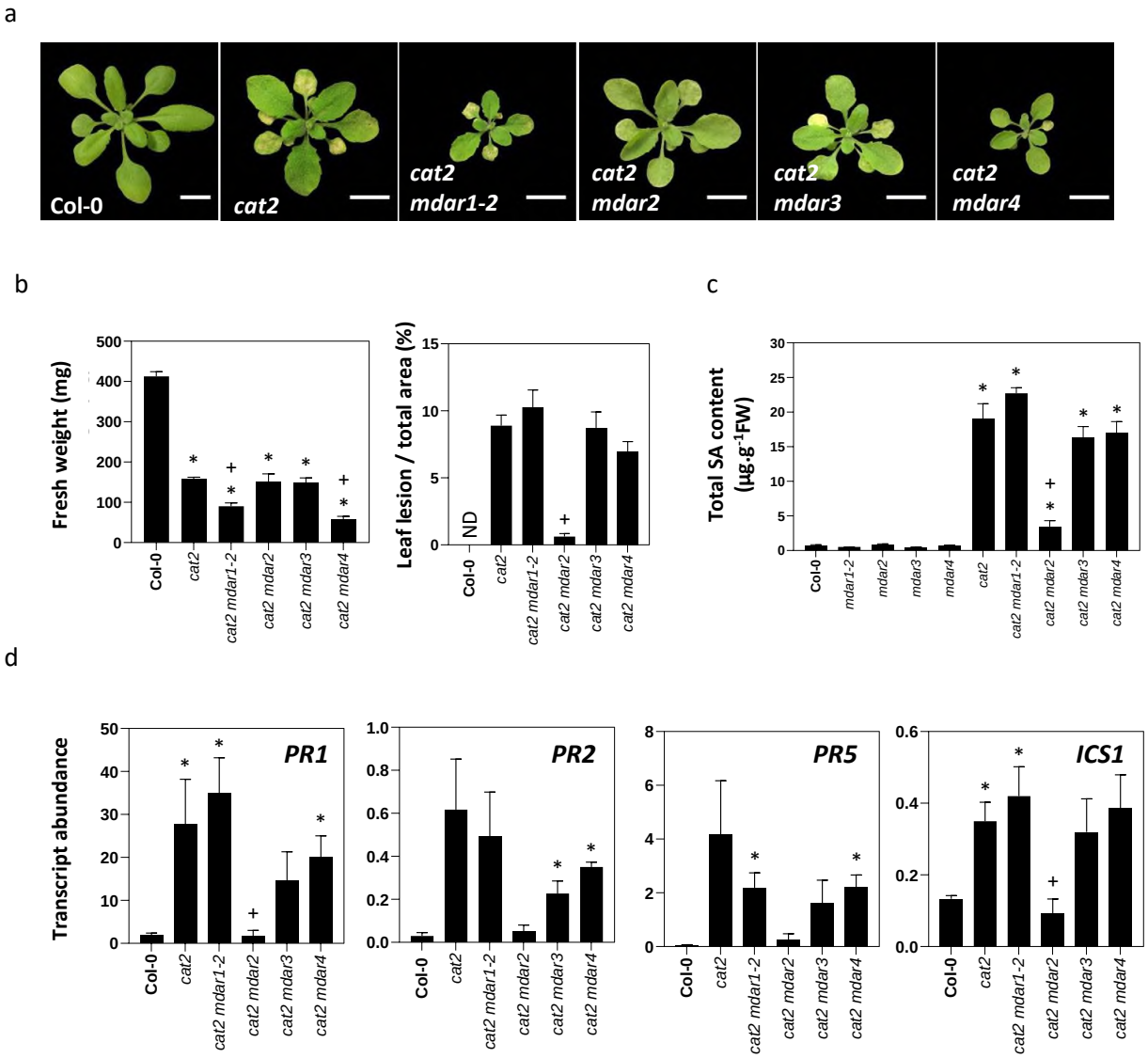

Figure 4. Effect of *mdar* mutations on the *cat2* phenotype and the SA pathway. a. Photographs of rosettes. b. Fresh weight and lesion quantification. Data are means ± SE of 10 plants. c. SA contents. d. *PR* gene expression. Data are means ± SE of three biological replicates. Student's t-test, *Significant difference compared to Col-0 at $P < 0.05$. $^{+}$Significant differences of double mutants compared with *cat2* at $P < 0.05$. Bars = 1 cm. ND: not detected.

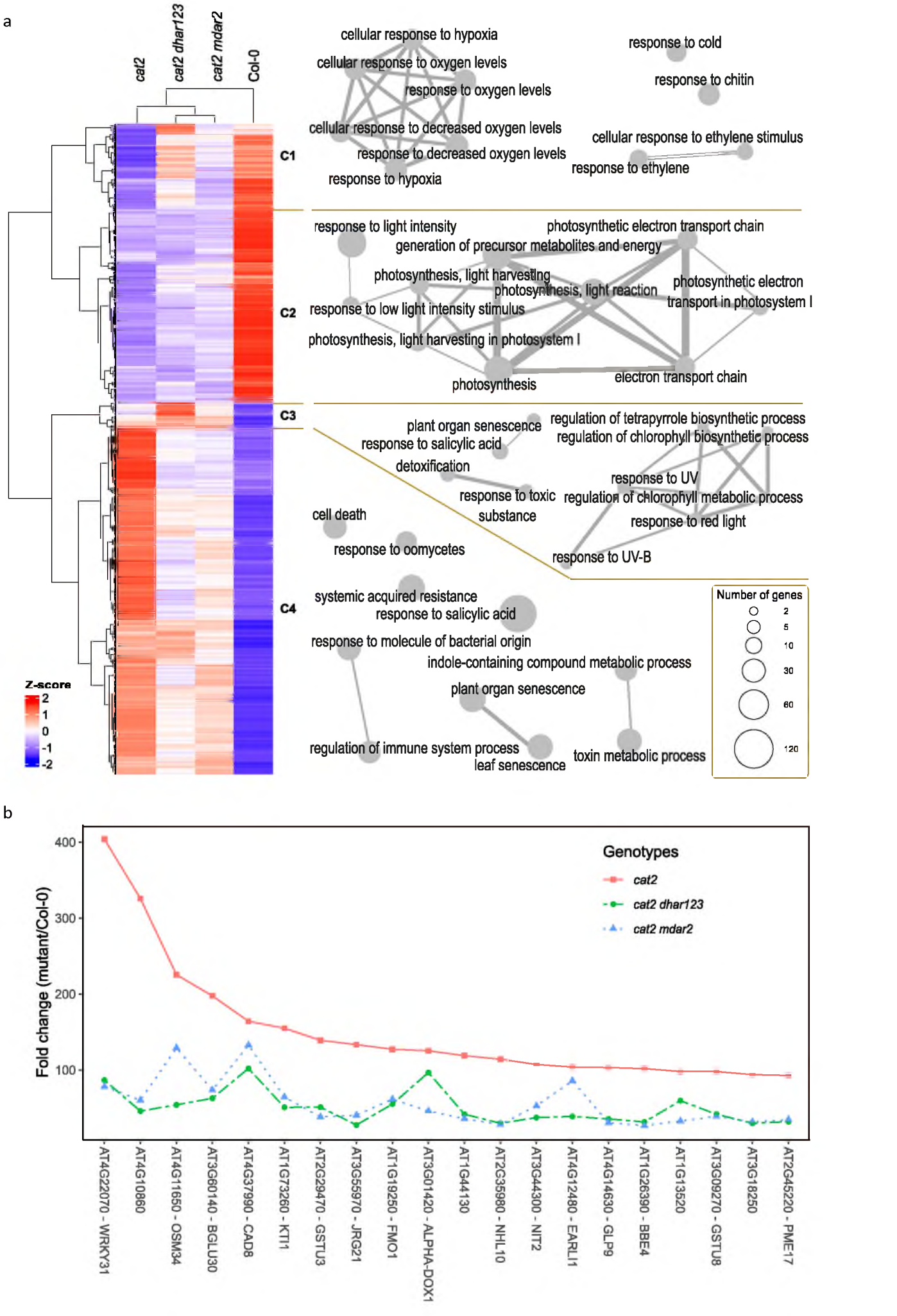
a
cat2
cat2 dhar123
cat2 mdar2
Col-0
C1
C2
C3
C4
Z-score
2
1
0
-1
-2
cellular response to hypoxia
cellular response to oxygen levels
response to oxygen levels
cellular response to decreased oxygen levels
response to decreased oxygen levels
response to hypoxia
response to cold
response to chitin
cellular response to ethylene stimulus
response to ethylene
response to light intensity
photosynthetic electron transport chain
generation of precursor metabolites and energy
photosynthesis, light harvesting
photosynthesis, light reaction
photosynthetic electron transport in photosystem I
response to low light intensity stimulus
photosynthesis, light harvesting in photosystem I
photosynthesis
electron transport chain
plant organ senescence
regulation of tetrapyrrole biosynthetic process
regulation of chlorophyll biosynthetic process
response to salicylic acid
detoxification
response to UV
response to toxic substance
regulation of chlorophyll metabolic process
cell death
response to red light
response to oomycetes
response to UV-B
systemic acquired resistance
response to salicylic acid
response to molecule of bacterial origin
indole-containing compound metabolic process
plant organ senescence
regulation of immune system process
leaf senescence
toxin metabolic process
Number of genes
2
5
10
30
60
120
b
Fold change (mutant/Col-0)
400
300
200
100
Genotypes
cat2
cat2 dhar123
cat2 mdar2
AT4G22070 - WRKY31
AT4G10860
AT4G11650 - OSM34
AT3G60140 - BGLU30
AT4G37990 - CAD8
AT1G73260 - KTI1
AT2G29470 - GSTU3
AT3G55970 - JRG21
AT1G19250 - FMO1
AT3G01420 - ALPHA-DOX1
AT1G44130
AT2G35980 - NHL10
AT3G44300 - NIT2
AT4G12480 - EARLI1
AT4G14630 - GLP9
AT4G26390 - BBE4
AT1G13520
AT3G09270 - GSTU8
AT3G18250
AT2G45220 - PME17

Figure 5. Transcriptomic analysis of *cat2*, *cat2 mdar2*, and *cat2 dhar1 dhar2 dhar3*. a. Heatmap showing normalized expression (Z-score of CPM) of the 1521 differentially expressed genes between Col-0 and *cat2* (FDR<0.01 & $|\log_2 FC|>1$). The top 10 of Biological Process GO enrichment for each of the 4 clusters is displayed on the right (p-adjust<0.05). The circle size corresponds to the number of DEGs responsible for the enrichment. A joining line indicates a link between GO terms. b. Effects of secondary mutations in ascorbate regeneration on the 20 genes with the highest fold change for *cat2* compared to Col-0. The fold change is calculated using mean CPM and Col-0 as reference.

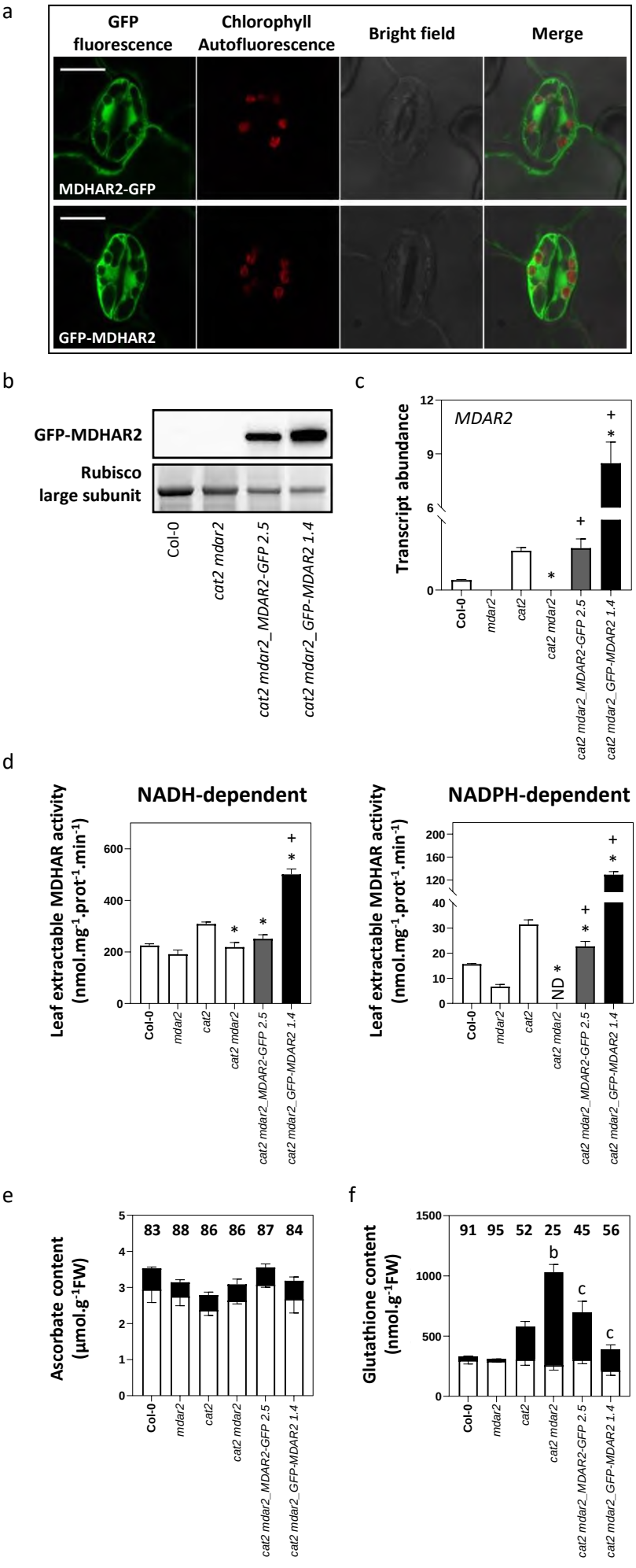
a
GFP fluorescence
Chlorophyll Autofluorescence
Bright field
Merge
MDHAR2-GFP
GFP-MDHAR2
b
GFP-MDHAR2
Rubisco large subunit
Col-0
cat2 mdar2
cat2 mdar2_MDAR2-GFP 2.5
cat2 mdar2_GFP-MDAR2 1.4
c
MDAR2
Transcript abundance
12
9
6
0
Col-0
mdar2
cat2
cat2 mdar2
cat2 mdar2_MDAR2-GFP 2.5
cat2 mdar2_GFP-MDAR2 1.4
d
NADH-dependent
Leaf extractable MDHAR activity (nmol.mg-1.prot-1.min-1)
600
400
200
0
NADPH-dependent
200
160
120
40
30
20
10
ND
e
Ascorbate content (µmol.g-1FW)
5
4
3
2
1
0
83 88 86 86 87 84
f
Glutathione content (nmol.g-1FW)
1500
1000
500
0
91 95 52 25 45 56
b
c
c

Figure 6. Complementation of *cat2 mdar2* with GFP-MDAR2. a. GFP analysis of subcellular localisation of MDHAR2. The bar indicates 10 µm. b. Verification of *MDAR2* expression in the complemented lines using an anti-GFP antibody. c. Verification of complemented *MDAR2* transcripts. d. Effects on MDHAR activities. e. Effects on ascorbate contents. Numbers above the bars indicate % reduction. f. Effects on glutathione contents. Numbers above the bars indicate % reduction. Data are means ± SE of three biological replicates. *Significant difference compared to *cat2* at $P < 0.05$. $^{+}$Significant differences of complemented lines compared with *cat2 mdar2* at $P < 0.05$. For c and d, the white columns represent untransformed lines, the grey column represents the C-terminal transformed line, and the black column represents the N-terminal transformed line. ND: not detected. In e and f, ^{b} indicates significant differences of oxidized forms in the double mutant compared with *cat2* at $P < 0.05$ and ^{c} indicates significant differences in oxidized forms of MDAR2 complemented lines compared with *cat2 mdar2* at $P < 0.05$.

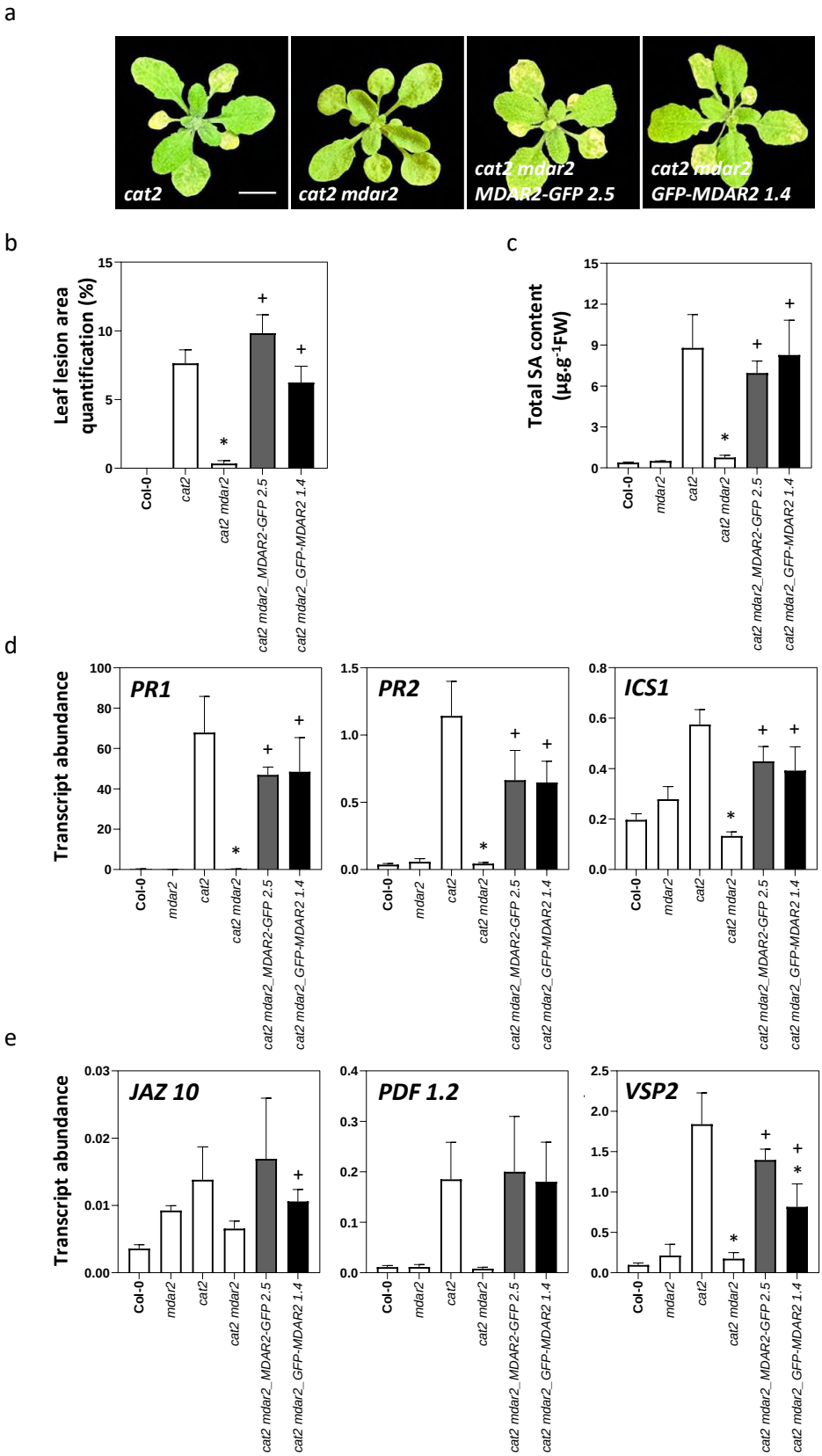

Figure 7. Complementation of *cat2 mdar2* with GFP-MDAR2 restores the *cat2* lesion phenotype and pathogenesis-related pathways. a. Phenotypes of complemented lines. b. Leaf lesion area quantification. c. SA contents. d. SA-related gene expression. e. JA-related gene expression. The white columns represent untransformed lines, the grey column represents the C-terminal transformed line, and the black column represents the N-terminal transformed line. *Significant difference compared to *cat2* at $P < 0.05$. $^{+}$Significant differences of complemented lines compared with *cat2 mdar2* at $P < 0.05$.

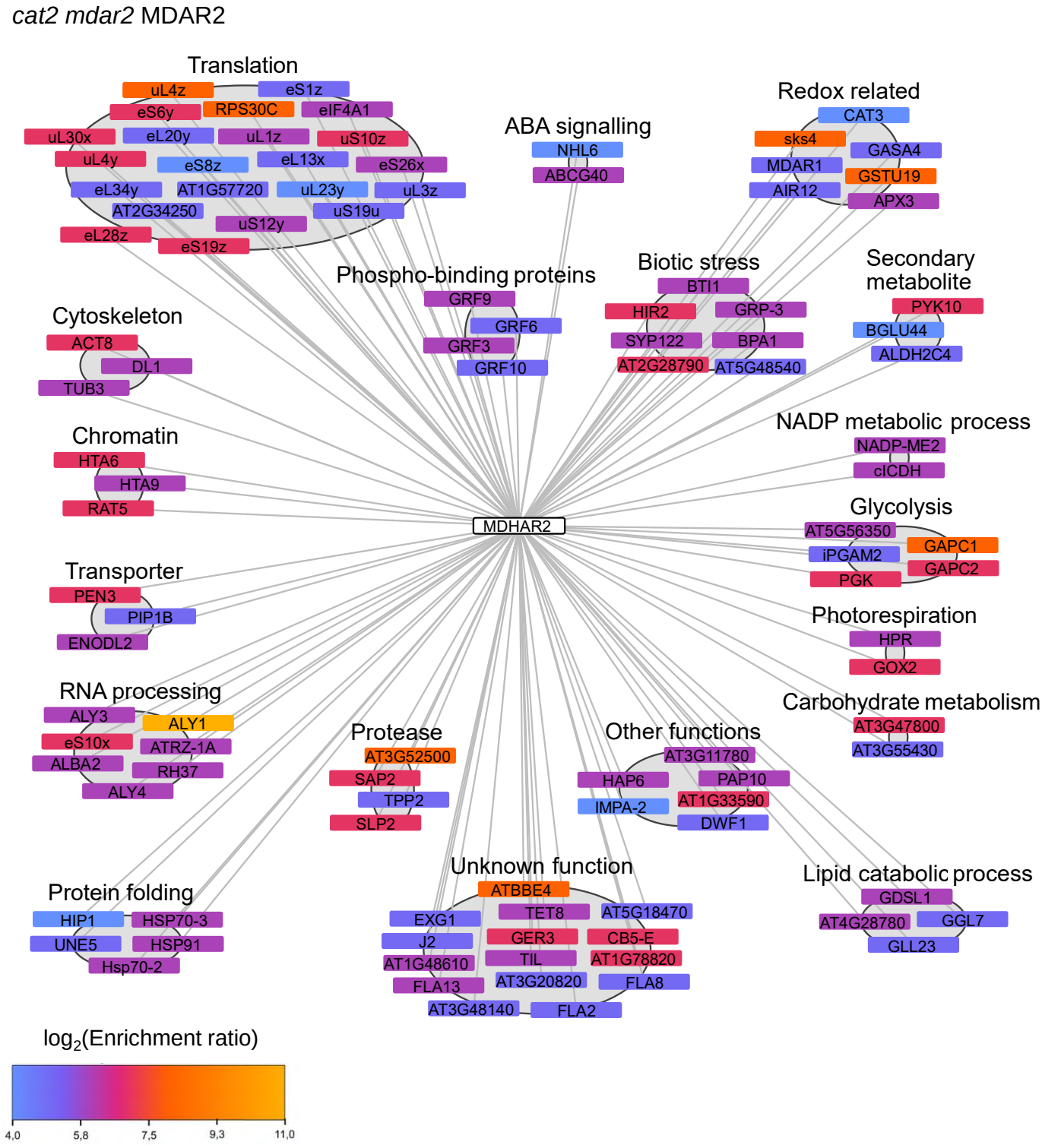

Figure 8. Overview of immunoprecipitation–mass spectrometry (IP-MS) search for protein interactants in *cat2 mdar2* MDAR2-GFP. The interactants shown have an enrichment ratio >25 and a p-value < 0.05. Proteins are grouped by biological processes. The box colour corresponds to the $\log_2$(enrichment ratio) with MDAR2 protein. For more details on proteins, see Supporting Information Table S3.

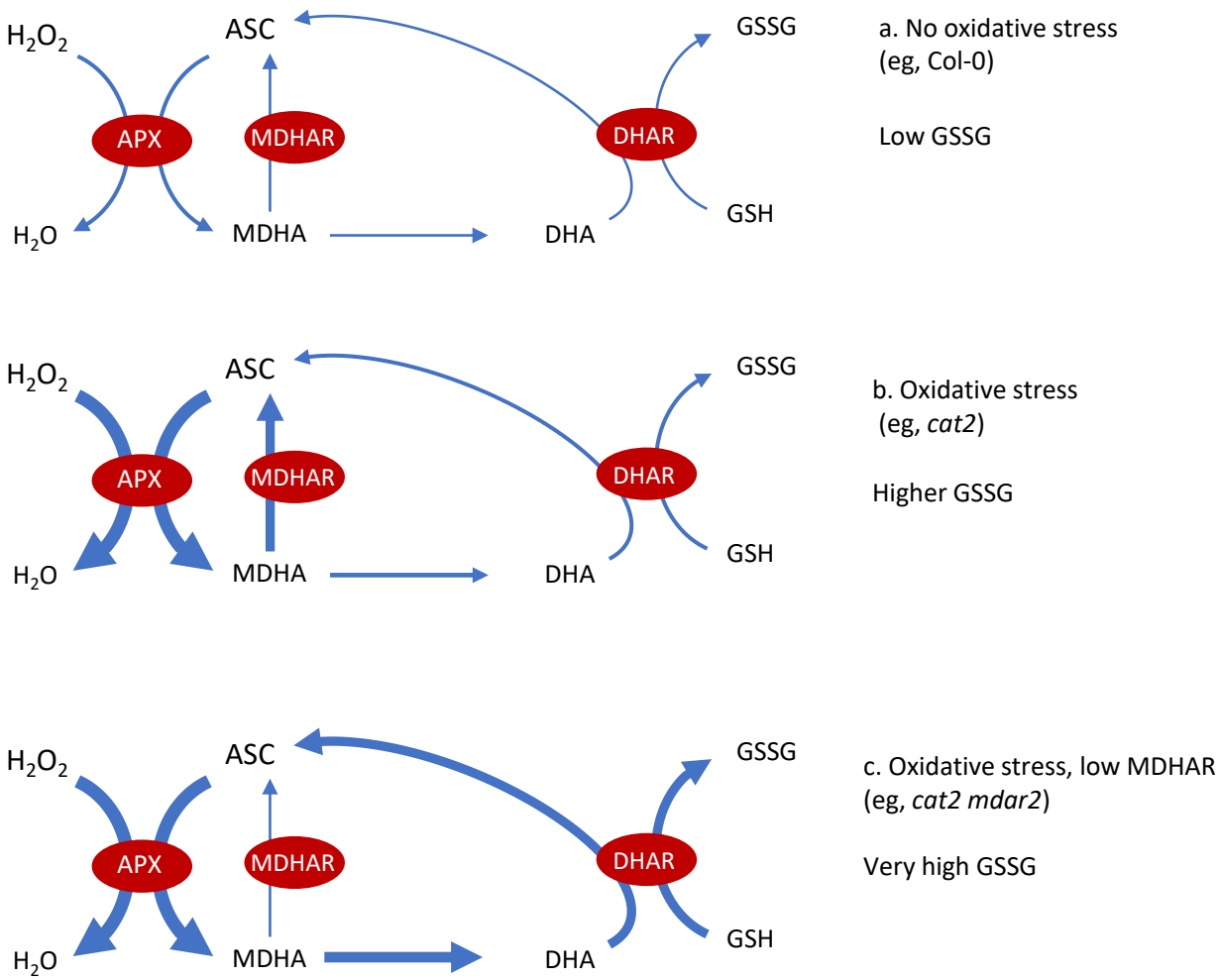

Figure 9. Impact of oxidative stress and MDHAR capacity on measured glutathione status. In conditions where H_2O_2 can be largely removed by catalase (a), flux through the ascorbate and glutathione pools is low and glutathione remains highly reduced. When catalase is decreased (b), flux through the ascorbate pool is increased, causing accelerated formation of both MDHA and DHA, with the latter engaging the glutathione pool, leading to GSSG accumulation. When flux is high and MDHAR is decreased (c), conversion of MDHA to DHA is increased compared to b and the glutathione pool is further engaged, leading to even higher GSSG accumulation. Note that the pathway is shown in simplified form and that reactions are not shown stoichiometrically.

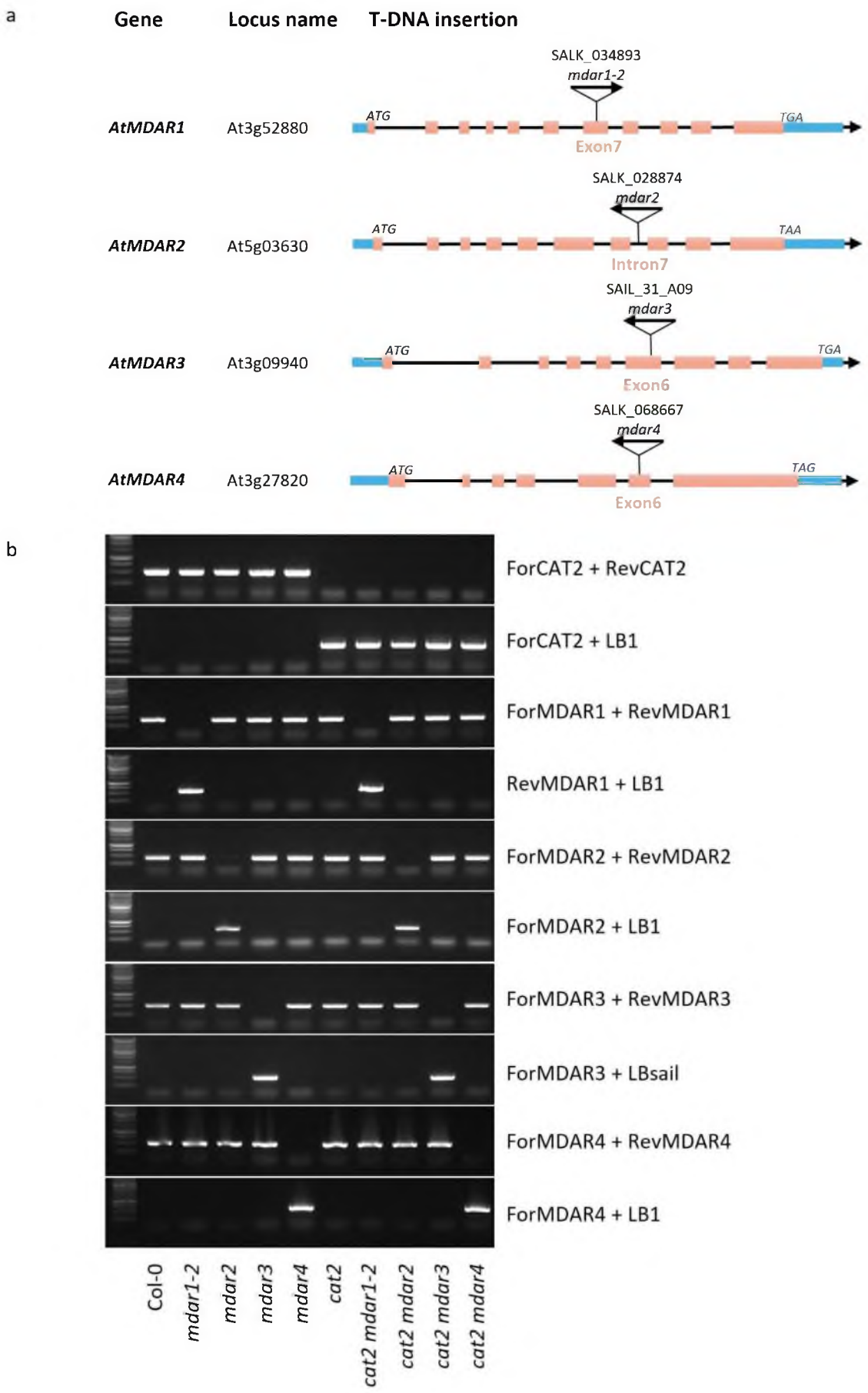

Supporting Information Figure S1. Gene maps (a) and genotyping (b) of *mdar* and *cat2 mdar* mutants.

a

b

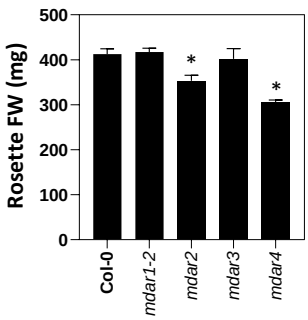

Supporting Information Figure S2. Effect of *mdar* mutations on plant growth in standard conditions. a. Photographs of *mdar* mutants. b. Rosette fresh weights. Data are means ± SE of 10 plants. Student's t-test * indicates significant differences of mutants compared with Col-0 at $P < 0.05$.

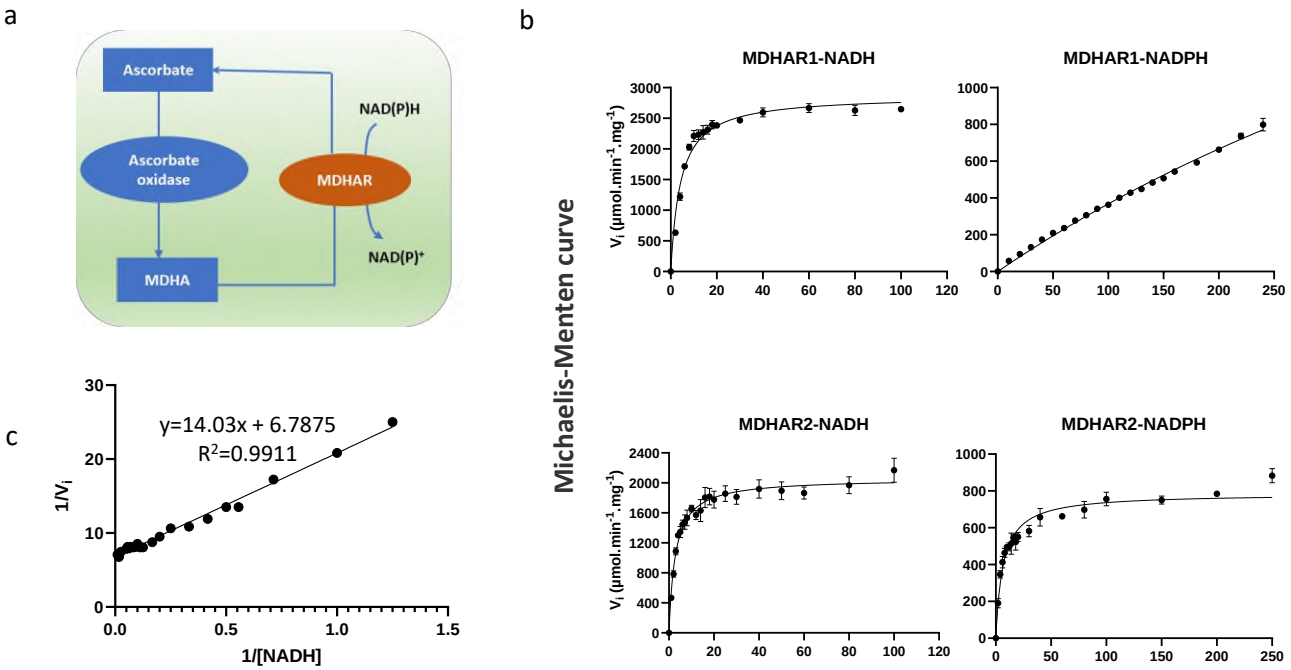

Supporting Information Figure S3. Enzyme parameters for MDHAR recombinant proteins. a. Principle of the MDHAR assay. b. Kinetic curves for MDHAR activity of recombinant proteins. c. An example of a Lineweaver-Burk plot for MDHAR.

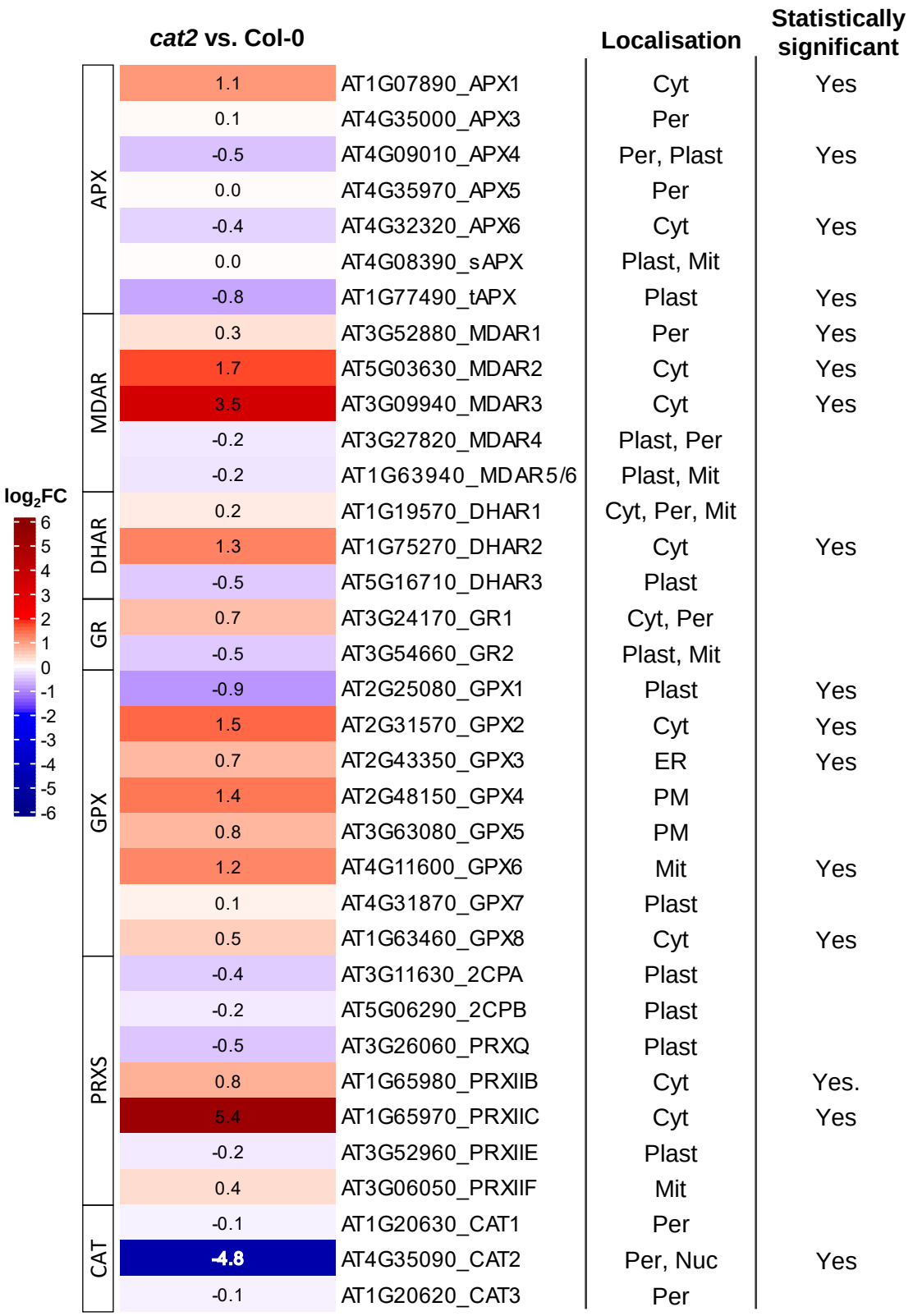

Supporting Information Figure S4. Effect of the *cat2* mutation on expression of some of the major H_2O_2 metabolizing pathways in Arabidopsis. Data are shown for genes encoding catalases (CAT), members of the ascorbate-glutathione pathway (MDAR, DHAR, GR), peroxiredoxins (PRXS) and glutathione peroxidase-like proteins (GPX). The heatmap display $\log_2$(foldchange) of the mean of CPM comparing *cat2* and Col-0. Only gene that could be quantified in both genotype are included. The major subcellular localisation is indicated according to SUBA5 consensus localisation and annotation from literature. Statistically significant differences between Col-0 and *cat2* at $P < 0.01$ are indicated as a "Yes". Cyt, cytosol. ER, endoplasmic reticulum. Mit, mitochondrion. Nuc, nucleus. Per, peroxisome. Plast, plastid. PM, plasma membrane

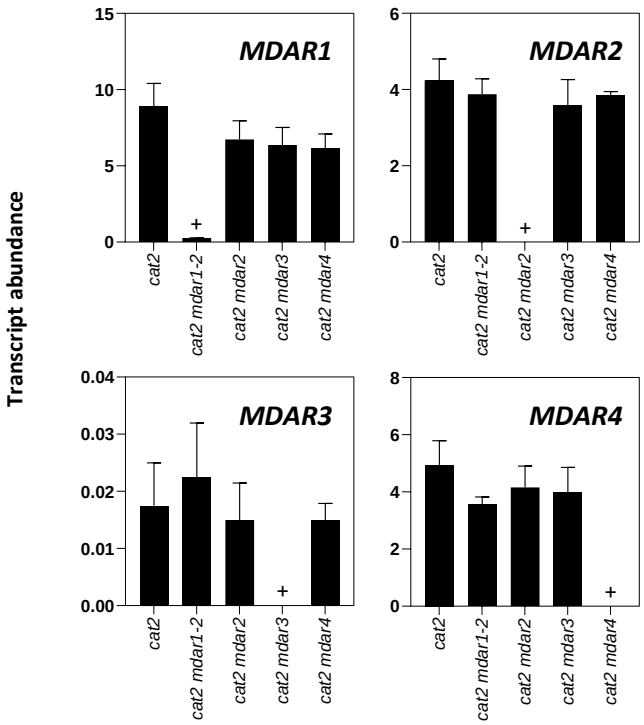

Supporting Information Figure S5. transcripts analysis of *MDAR* gene in *cat2* background, using *ACTIN2* and *PP2A* are reference genes. Data are means ± SE of three biological replicates. Studient's t-test, + indicates significant differences of double mutants compared with *cat2* at $P < 0.05$